Journal of Hydrology 510 (2014) 228–245

Contents lists available at ScienceDirect

Journal of Hydrology

journal homepage: www.elsevier.com/locate/jhydrol

Physically-based extreme flood frequency with stochastic storm transposition and paleoflood data on large watersheds

John F. England Jr. [a,*], Pierre Y. Julien [b], Mark L. Velleux [c]

[a] Bureau of Reclamation, Flood Hydrology, 86-68250, Denver Federal Ctr., Denver, CO 80225, USA
[b] Department of Civil Engineering, Colorado State University, Fort Collins, CO 80523, USA
[c] HDR—HydroQual, Inc., Mahwah, NJ 07430, USA

ARTICLE INFO

Article history:
Received 23 February 2013
Received in revised form 16 August 2013
Accepted 10 December 2013
Available online 16 December 2013
This manuscript was handled by Andras Bardossy, Editor-in-Chief, with the assistance of Ezio Todini, Associate Editor

Keywords:
Extreme floods
Flood probabilities
Distributed runoff
Paleofloods
Dam safety

SUMMARY

Traditionally, deterministic flood procedures such as the Probable Maximum Flood have been used for critical infrastructure design. Some Federal agencies now use hydrologic risk analysis to assess potential impacts of extreme events on existing structures such as large dams. Extreme flood hazard estimates and distributions are needed for these efforts, with very low annual exceedance probabilities ($\leqslant 10^{-4}$) (return periods >10,000 years). An integrated data-modeling hydrologic hazard framework for physically-based extreme flood hazard estimation is presented. Key elements include: (1) a physically-based runoff model (TREX) coupled with a stochastic storm transposition technique; (2) hydrometeorological information from radar and an extreme storm catalog; and (3) streamflow and paleoflood data for independently testing and refining runoff model predictions at internal locations. This new approach requires full integration of collaborative work in hydrometeorology, flood hydrology and paleoflood hydrology. An application on the 12,000 km^2 Arkansas River watershed in Colorado demonstrates that the size and location of extreme storms are critical factors in the analysis of basin-average rainfall frequency and flood peak distributions. Runoff model results are substantially improved by the availability and use of paleoflood nonexceedance data spanning the past 1000 years at critical watershed locations.

Published by Elsevier B.V.

1. Introduction

The estimation of extreme flood probabilities is a long-standing problem in hydrology, because we typically lack long flood records (Stedinger et al., 1993) to estimate Annual Exceedance Probabilities (AEPs) at the site of interest. About a century ago, Hazen (1914) recognized the practical value of this problem and suggested the idea of unbounded, very extreme flood probabilities when commenting on Fuller (1914): "... One of the most important matters developed by the paper is that there is no such thing as a maximum flood. ... There is a 100-year flood much greater than the 10-year flood; and, although no records are at hand to demonstrate it adequately, there is every reason to believe that there is a 1000-year flood, which will prove to be much greater than the 100-year flood." Several years later, the value of geologic information and terraces for flood information was recognized (Fuller (1917); see also Jarrett and England (2002) for a discussion). Today, paleoflood data with records longer than 1000 years (House et al., 2002; Levish, 2002; Benito et al., 2005) are now available or can be obtained for extreme flood frequency analysis (O'Connell et al., 2002; England et al., 2010), and provide crucial data for temporal extension of flood information (e.g. Merz and Blöschl, 2008a).

In contrast to widely-used deterministic design procedures for large dams and critical infrastructure, such as the Probable Maximum Flood (PMF) (Cudworth, 1989), methods to estimate extreme floods, extreme rainfalls and their probabilities are not mature (NRC, 1988, 1994; Burges, 1998). Estimates of extreme floods and AEPs are needed and required for hydrologic engineering, dam safety risk analysis and modification of critical infrastructure, particularly by the Bureau of Reclamation (Reclamation, 2010, 2011). The hydrologic hazard inputs required for risk analysis are frequency distributions of peak flows, hydrographs, volumes, and peak reservoir stages which, for dams with potentially high loss of life, extends to very low AEPs ($\leqslant 10^{-4}$). In practice, there are few readily-available tools to make these estimates. Some methods to estimate hydrologic hazards for dam safety with AEPs $\leqslant 1/2000$ are described by Nathan and Weinmann (1999) for Australia and by Swain et al. (2006) for Reclamation dams in the western US. In Germany and Austria, DWA (2012) provides hydrologic hazard methods for dam safety that explicitly focus on temporal, spatial, and causal information to complement the systematic flood data. Tools generally consist of peak-flow frequency with paleoflood data (O'Connell et al., 2002), lumped unit hydrograph (HEC, 2010) or storage routing models (Laurenson et al., 2006), with rain-

* Corresponding author. Tel.: +1 303 445 2541.
E-mail addresses: jengland@usbr.gov (J.F. England Jr.), pierre@engr.colostate.edu (P.Y. Julien), mark.velleux@hdrinc.com (M.L. Velleux).

0022-1694/$ - see front matter Published by Elsevier B.V.
http://dx.doi.org/10.1016/j.jhydrol.2013.12.021

fall probabilities estimated with L-Moments (Hosking and Wallis, 1997) or AEP shape functions based on Probable Maximum Precipitation (PMP) (Nathan and Weinmann, 1999). The GRADEX method (Naghettini et al., 1996; Swain et al., 2006; Gutknecht et al., 2006) is also used in some cases. Reclamation utilizes paleoflood data to estimate hydrologic hazard curves for risk analyses, which includes risk-based modifications at major facilities in California (Reclamation, 2002) and Wyoming (Levish et al., 2003). Others (Schumann, 2010) are also examining extreme flood hazard issues. There is much room for conducting innovative extreme flood hydrology science, engineering, and applications in this challenging area to estimate AEPs $\leqslant 10^{-4}$.

This paper presents an integrated data-modeling hydrologic hazard framework for detailed, physically-based extreme flood hazard estimation. The framework is suitable for hydrologic risk applications for critical infrastructure such as dams and nuclear reactors; we show an example for a large dam in the Western United States. We implement several extreme flood and rainfall concepts presented in NRC (1988, 1994), including stochastic storm transposition (Foufoula-Georgiou, 1989) and paleoflood data (House et al., 2002). The hydrologic hazard framework consists of the following key elements: (1) rainfall frequency and storm modeling with stochastic storm transposition; (2) extreme storm data and analyses for storm probability modeling supplemented by radar data; (3) physically-based rainfall–runoff modeling with the Two-Dimensional Runoff, Erosion and Export (TREX) model (Velleux et al., 2011) to estimate flood frequency; and (4) streamflow and paleoflood data with frequency analysis utilized for independently testing and refining runoff model predictions. We demonstrate the approach on a large 12,000 km^2 watershed, the Arkansas River above Pueblo, Colorado, to estimate the flood hazard at Pueblo Dam, a Bureau of Reclamation water-supply and flood control dam.

The study objectives are: (1) implement and demonstrate the use of stochastic storm transposition (SST) on a large, orographic watershed; (2) utilize a physically-based runoff model (TREX) with spatially and temporally distributed rainfall from stochastic storm transposition to estimate flood frequency on this watershed; and (3) examine effects of varying spatial rainfall and soil moisture on flood frequency curves, comparing model predictions to streamflow and paleoflood data at internal watershed locations. We build on previous studies, including TREX development (England et al., 2007), storm hydrometeorology (Javier et al., 2007), and paleoflood data and frequency analysis (England et al., 2010).

2. Hydrologic hazard framework for large, semi-arid watersheds

The hydrologic hazard framework is designed to provide information on hydrologic risk – very extreme floods with AEPs $\leqslant 10^{-4}$ – that is required for making dam safety decisions (Reclamation, 2011). This information includes peak-flow frequency and hydrographs for large (>5000 km^2), semi-arid watersheds. The framework utilizes two methods to estimate the hydrologic hazard (NRC, 1988): peak-flow frequency using a statistical model with paleofloods; and rainfall–runoff modeling with extreme storms. The statistical model for peak-flow frequency that is used in this study is the log-Pearson Type 3 (LP3) distribution with the Expected Moments Algorithm (EMA) (Cohn et al., 1997) and confidence intervals (Cohn et al., 2001). The physically-based rainfall–runoff model TREX (England et al., 2007; Velleux et al., 2008, 2011) is coupled with SST and extreme storm data to estimate flood frequency and hydrographs. These two methods are used in a combined way. TREX provides a physical basis for flood hydrographs; the model predictions are compared with the independent EMA-LP3 flood frequency (using peak-flow and paleoflood data) and refined as needed.

We directly account for the following key physical processes (see England (2006) and England et al. (2007) for a discussion and review) in the rainfall–runoff model component of the hydrologic hazard framework: (1) extreme storm rainfall (duration, spatial pattern, location, areal extent); (2) partial-area rainfall and runoff; (3) hillslope runon, runoff and routing; and (4) channel network and routing. There are significant research opportunities on the extreme flood physical processes and flood frequency using physically-based rainfall–runoff models for large watersheds, as most approaches have been statistically-based (Dunne, 1998). On large basins >10^3 km^2, watershed response is controlled by travel time in channels and by the specifics of the spatial distribution of rainfall (Nicótina et al., 2008). Partial-area rainfall and runoff dynamics play a crucial role in semi-arid regions (Marco and Valdés, 1998; Iacobellis and Fiorentino, 2000; Fiorentino and Iacobellis, 2001; Moon et al., 2004) at these scales. We use the TREX model to represent these physical processes in a spatially-distributed manner, especially partial-area rainfall and channel routing.

Extreme storm rainfall data, flood data, and paleoflood data are a critical part of the hydrologic hazard framework. As noted by NRC (1988), major efforts are needed to compile comprehensive data bases for developing and testing extreme flood probability methods. The following data sets are utilized in this framework. Extreme storm rainfall are obtained from USACE (1973), Hansen et al. (1988), NOAA NCDC data bases, Reclamation's extreme storm files (Sankovich and Caldwell, 2011), and newer storms from site-specific data collection efforts (Section 4.2). Extreme flood data (peak flows, daily flows, hydrographs) are obtained from the USGS NWIS and related flood publications (Follansbee and Jones, 1922; Follansbee and Sawyer, 1948). Historical data and paleoflood data are obtained on a site-specific and regional basis (Klinger and Klawon, 2002). For this study we rely on detailed, site-specific and regional data collection efforts on extreme storms and paleofloods for the flood hazard at Pueblo Dam. When combined, these data sets provide a basis for extrapolation to AEPs of interest (Swain et al., 2006). England (2011) describes ongoing improvements to extreme storm, flood, and paleoflood data bases within the U.S.

Few published studies provide approaches to estimate extreme flood probabilities (AEPs $\leqslant$ 1/1000) with rainfall–runoff models. Recent efforts are summarized in Table 1, and most use an exponential storm model with TOPMODEL. Our watershed scales of interest are 10–100 times larger than these past studies. Most of these studies use a single method, rather than the two approaches in the present work. While Cameron (2007) and Rogger et al. (2012) compared runoff model estimates with independent peak-flow frequency curves, we use paleoflood data that these studies did not consider. We are also motivated to use a different hydrologic hazard framework than these previous studies based on the following considerations. We implement the NRC (1994) recommendation to use storm-based analysis of extreme rainfall with SST (Section 4), because the data base and model provide direct information on largest rainfalls and the upper tail of the basin-average precipitation frequency curve. The SST approach can also include partial-area rainfall effects. The TREX model (Section 5) is utilized to represent the important physical watershed processes, interactions and dynamics of extreme floods in a spatially-explicit manner: the location, orientation and spatial distribution of rainfall (England et al., 2007); runoff from hillslopes (2D diffusive-wave routing); and channel network and hydraulics (1D diffusive-wave routing). While there may be several open research questions regarding storm rainfall and runoff model complexity for these extreme flood hazard problems, we present this framework as one alternative. It is hoped that this study might be used to motivate additional research work in this challenging area.

Table 1
Recent extreme flood frequency studies using rainfall–runoff models, with AEPs ⩽ 0.001 (modified from Beven (2001) and England (2006)).

Study	Catchment	Area (km^2)	Rainstorm model	Runoff generation	Routing	AEP
Cordova and Rodriguez-Iturbe (1983)	Quercual, Venezuela	250	Observed	Hortonian Infiltration Excess	GUH	1/1000
Franchini et al. (1996)	hypothetical midwest US	–	Stochastic Storm Transposition	ARNO	Parabolic	1/100,000
Cameron et al. (1999)	Wye, UK	10.6	GPD extension to observed	TOPMODEL	Linear NWF	1/1000
Hashemi et al. (2000)	hypothetical	100	Modified Neyman-Scott	ARNO	Parabolic	1/10,000
Cameron et al. (2000)	4 gaged UK catchments	0.9–415.6	GPD extension to observed	TOPMODEL	Linear NWF	1/1000
Blazkova and Beven (2002)	Joseful Dul, Czech Rep.	25.8	Modified Eagleson	TOPMODEL	Linear NWF	1/10,000
Blazkova and Beven (2004)	Zelivka, Czech Rep.	1186	Modified Eagleson	TOPMODEL	Network constant velocity	1/10,000
Struthers and Sivapalan (2007)	Hypothetical	–	Exponential	Conceptual single bucket subsurface and surface	None	1/1000
Cameron (2007)	Findhorn, UK	415.6	GPD extension to observed	TOPMODEL	Linear NWF	1/1000

GPD, Generalized Pareto Distribution; GUH, geomorphological instantaneous unit hydrograph; NWF, network width function.

This hydrologic hazard framework integrates temporal, spatial and causal flood hydrology information, in the spirit of Merz and Blöschl (2008a,b):

1. temporal: extreme storms, paleoflood and historical peak-flow data (England et al., 2010);
2. spatial: extreme storms within region (transposition) and spatial storm models conditioned by radar information (Javier et al., 2007); and
3. causal: flash floods, partial-area rainfalls, elevation limits that affect the spatial extent of extreme storms (Jarrett, 1993; England et al., 2010), paleofloods and snowmelt processes.

The framework requires full integration of collaborative work in hydrometeorology, flood hydrology and paleoflood hydrology. The Arkansas River basin application is used as an example to demonstrate the approach, because extreme flood data, channel properties, paleoflood data, and regional extreme storm rainfall data were specifically collected for the analysis.

3. Arkansas River basin flood hydrology overview

The study watershed for demonstrating flood frequency with stochastic storm transposition and paleoflood data is the 12,000 km^2 Arkansas River basin in southeastern Colorado (Fig. 1). The 76 m high Pueblo Dam and 440 million m^3 reservoir are the major features of the Bureau of Reclamation's Fryingpan-Arkansas project (Water and Power Resources Service, 1981), and are located just upstream of Pueblo, Colorado. The salient extreme flood hydrology-related features of this large watershed include: (1) mixed-population flood runoff mechanisms from snowmelt and rainfall excess (England et al., 2006, 2010); (2) complex topography and orography influencing storm rainfall (Javier et al., 2007); and (3) a history of extreme floods, including the devastating 3–4 June 1921 flood that killed over 120 people (Follansbee and Jones, 1922; Munn and Savage, 1922). The watershed is surrounded by some of the highest peaks and ranges in the Conterminous US, including the Collegiate Peaks (central Sawatch Range), Mosquito Range, Sangre de Cristo mountains, Wet mountains, and Pikes Peak. Elevations within the watershed range from 4400 m (Mt. Elbert) to 1490 m (Pueblo Dam), with many peaks exceeding 4270 m. The topography and elevation changes within and surrounding the watershed play a key role in the flood hydrometeorology (Follansbee and Sawyer, 1948; Javier et al., 2007), severely limiting extreme storm propagation within the highly-confined upper portions of the watershed near Leadville.

The Arkansas River basin exhibits both regional and local physical controls to flood processes and typology, as reflected in peak-flow and rainfall data sets. The watershed encompasses three flood runoff zones: a snowmelt zone; a transition (snowmelt to rainfall) zone; and a rainfall zone (Fig. 1). The zones integrate the effects of drainage area, river network, elevation, topography, streamflow, and storm rainfall (England et al., 2006). Peak-flow generation from the high elevation sites, generally above 2300 m including near Leadville and Salida, is from snowmelt runoff in May and June, with high correlation between sites. At locations within the transition zone, peak flows are from snowmelt runoff, rainfall–runoff, or some combination. Peak flows in the lower, eastern portion of the watershed are predominately from rainfall–runoff, with flows nearly uncorrelated between the sites. A critical factor is snowmelt runoff at high elevations in the snowmelt zone (Fig. 1), and partial-area extreme rainfalls causing floods in the lower portion of the basin. Flood-peak histograms and individual flood hydrographs shown in England (2006) illustrate this effect. Regional peak flows are strongly influenced by elevation, and unit peak discharges dramatically decrease over short distances as elevations increase (Jarrett, 1987, 1990; England et al., 2010). This peak-flow based elevation limit hypothesis is a critical factor for flood frequency within this watershed, with regional unit peak discharges dramatically decreasing to <20 $m^3/s/km^2$ for elevations >2300 m (Jarrett, 1993; England, 2006). At lower elevations, unit peak discharges are significantly higher (see Fig. 3 in England et al. (2010)), approaching 140 $m^3/s/km^2$ for convective rainfalls over small areas. Historical peak-flow and paleoflood data (England et al., 2010) provide both temporal and spatial expansions (Merz and Blöschl, 2008a) of flood peak-flow data at four sites within the Arkansas watershed (Fig. 1), and are crucial for independently testing flood frequency prediction from rainfall–runoff models (Section 5).

Storm precipitation over the Arkansas River watershed in March through June can result in significant rainfalls and large floods. These mid-latitude systems cross the region, strengthen on the leeward side of the Rockies and draw Gulf of Mexico moisture from the southeast into eastern Colorado. This moisture and increased convective activity result in periodic, widespread rainfall and occasionally severe thunderstorms east of the mountains

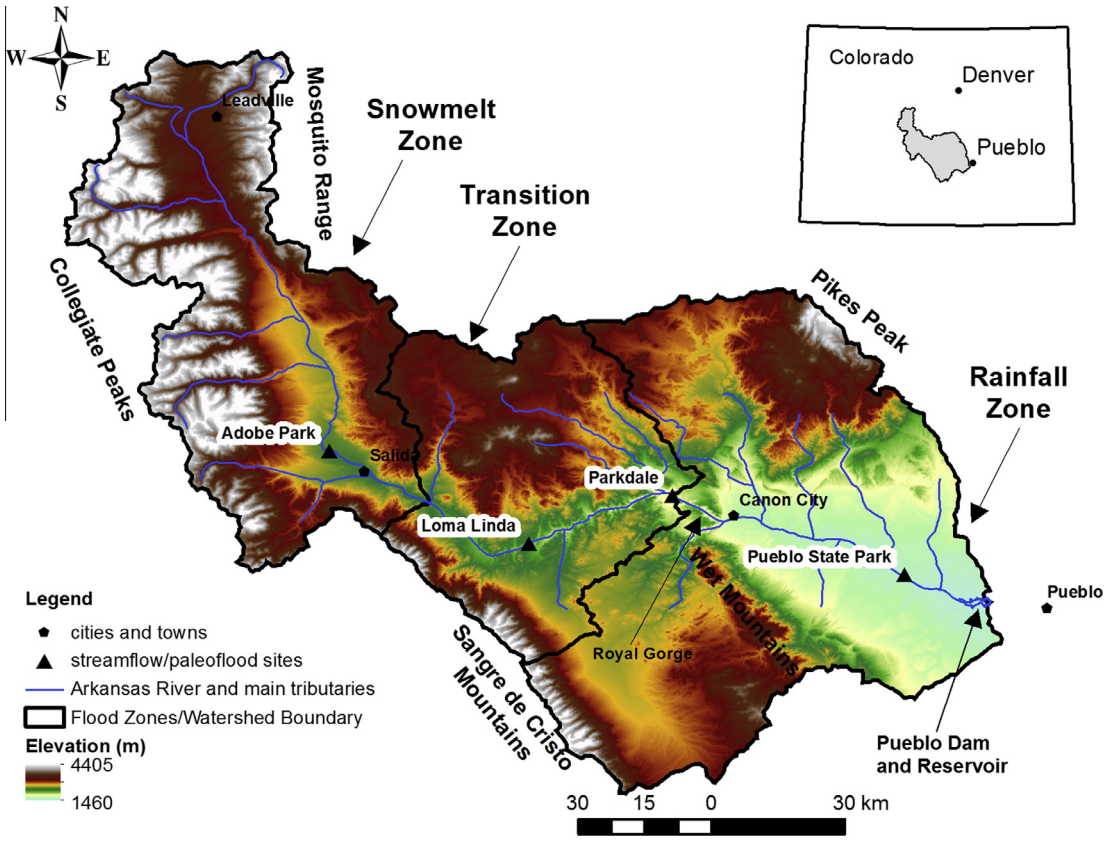

Fig. 1. Arkansas River watershed overview, showing topography, mountain ranges, and flood typology zones. Key streamflow and paleoflood sites from England et al. (2010) are shown as black triangles.

(Doesken, 1991). Similar to peak flows, storm rainfall amounts based on WSR-88D and cloud-to-ground lightning data show marked decreases with elevation (Javier et al., 2007). Importantly, the largest flood-producing extreme storms in the watershed (May 1894 and June 1921) initiated over lower portions of the watershed (England et al., 2007). Storm initiation sites are predominately along Pikes Peak and the Wet Mountains (Fig. 1), and storm activity is highest in this area. From analyses of 66 storm events, the upper portion of the Arkansas River basin does not contribute significantly to extreme flood peaks at Pueblo (Javier et al., 2007). Spatial evidence of storm activity is used to constrain extreme storm locations in the SST model.

4. Stochastic storm transposition

An extreme storm model is presented that is used to estimate basin-average extreme rainfall depths and AEPs with SST. Storm transposition is a regionalization concept that involves relocating individual storm precipitation within a region (considered homogeneous relative to topographic and meteorologic characteristics deemed significant to that storm) to a watershed of interest, greatly increasing the data available for evaluating the rainfall potential for a drainage (Schreiner and Riedel, 1978; Cudworth, 1989). Stochastic storm transposition is a generalization of the concept of storm transposition that is used to estimate PMP in the United States (e.g., Hansen et al., 1988). In the PMP application, storm transposition is based on the assumption that there exist meteorologically homogeneous regions such that a major storm occurring somewhere in the region could occur anywhere else in the region, with the provision that there may be differences in the averaged depth of rainfall produced based upon differences in moisture potential (NRC, 1988; Cudworth, 1989). Stochastic storm transposition extends this concept by incorporating the probability of occurrence (Fontaine and Potter, 1989). The at-site storm record within a watershed is significantly extended by using data from the surrounding region. Using the regional storm data, the hydrologist is substituting space for time, one of the three principles to improve extreme flood probability estimates (NRC, 1988). The regional data of given length are effectively equivalent to a much longer record at the watershed of interest.

Transposition concepts are illustrated in Fig. 2. The storm transposition area A_{tr} is the area within which all the occurred storms with storm area A_s can be transposed anywhere in the region either with the same depths and an adjustment to their probability of occurrence, or with the same probability of occurrence but with an adjustment to their depths (Foufoula-Georgiou, 1989). The interaction of storm area A_s with the watershed area A_c is an important feature of the approach, as partial-area rainfalls are accounted for depending on the transposed storm center location (x_s, y_s) and storm orientation θ. Storm areas within the watershed can also be restricted to account for elevation and process (snowmelt and rainfall) considerations (Fig. 2).

4.1. Storm model features

The general approach for stochastic storm transposition consists of two main parts: (1) estimating a basin-average maximum depth of storm rainfall $\bar{d}_c$ over a particular watershed with area A_c during a time period Δt and (2) estimating the cumulative probability distribution function (cdf) of the basin-average depth $F_{\bar{d}_c(\Delta t)}$ during that time period. The cdf of $\bar{d}_c$ depends on the joint distribution of the storm properties and the storm position (x, y). For conceptual understanding, one can consider this joint distribution in two parts: a "transposition" probability P_t that represents the

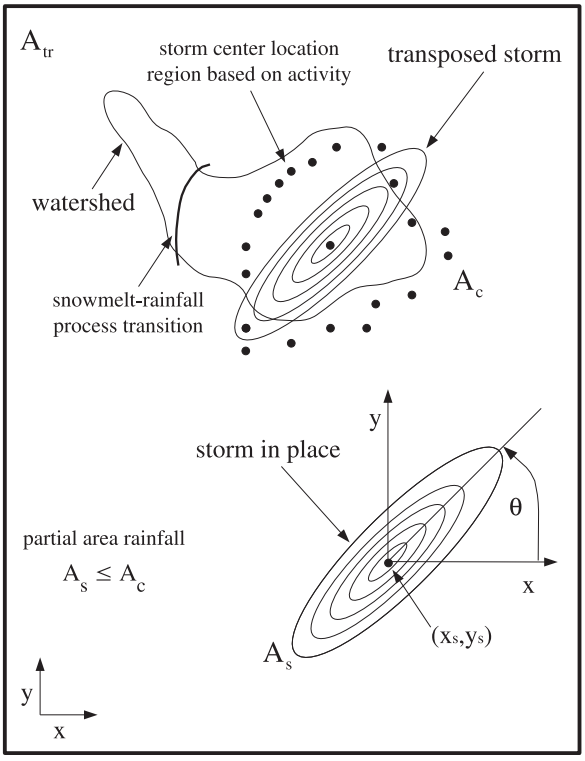

Fig. 2. Storm transposition concepts, showing transposition area A_{tr}, watershed area A_c, storm area A_s, storm orientation θ, storm center location (x_s, y_s), and flood process transition line.

probability of a storm center (x, y) falling within or near the watershed of interest; and a probability of occurrence P_r of a storm with depth that exceeds some minimum depth or rank in one year (Alexander, 1963).

The theoretical framework for the SST probability model that is used here is adopted from Foufoula-Georgiou (1989) and Wilson and Foufoula-Georgiou (1990). The SST model describes the AEP G^a of the maximum basin-average depth $\bar{d}_c(\Delta t)$ over a watershed. Annual probabilities are estimated, using data from an extreme storm catalog, by counting the number of extreme storms N_s in an interval of t years within a transposition region, with a discrete summation over actual storms (Foufoula-Georgiou, 1989):

$$G^a(d) = p_a(\bar{d}_c(\Delta t) \geqslant d) = \hat{p}_s \sum_{j=1}^{N_s} \hat{p}_j(\bar{d}_c(\Delta t) \geqslant d)\left(\frac{A_{eff\,j}}{A_{tr}}\right), \quad (1)$$

where $\hat{p}_s$ is the storm occurrence probability estimate for the region, $A_{eff\,j}$ is the effective area of the jth storm, A_{tr} is the transposition region, and $p_j(\bar{d}_c \geqslant d)$ is the probability for the jth storm that the average depth over the watershed is greater than some value d. This model provides basin-average extreme-storm rainfalls and AEPs in the range of interest ($\leq 10^{-4}$), as it combines the probabilities of transposition and occurrence. The maximum areally averaged rainfall depth $\bar{d}_c(\Delta t)$ that can occur over a watershed of area A_c during a time period Δt is estimated via:

$$\bar{d}_c(\Delta t) = \frac{1}{|A_c|}\int\int_{Ac}[d(x, y, t_s + \Delta t) - d(x, y, t_s)]dxdy, \quad (2)$$

where $\bar{d}_c$ is the maximum areally-averaged depth, (x, y) are spatial coordinates and Δt is a critical duration of rainfall in terms of flood production. This critical duration may be a fixed time period such as 6, 12, 24 or 72 h, up to a total storm duration t_s. For this study, estimates of $\bar{d}_c$ and t_s are obtained directly from depth-area duration (DAD) analyses of extreme storms from the storm catalog.

The major factors in (1) are the number of storms N_s, $\hat{p}_s$ and $A_{eff\,j}$. The effective area is defined as the area within which each storm must be centered and still cover at least one point within the watershed (Wilson and Foufoula-Georgiou, 1990) for runoff generation. This definition includes extreme rainfall depths for storms centered outside the watershed that partially cover or fully cover the watershed. The storm effective area changes every time a new storm is simulated over the watershed.

An important step in SST is the storm selection in order to obtain a complete catalog of all extreme storms that exceed a particular depth. A storm severity criterion E is used to select storms (Wilson, 1989):

$$\textit{Criterion } E: \quad \{\bar{d}[\Delta t, A] \geqslant d_{min}\}, \quad (3)$$

where $\bar{d}[\Delta t, A]$ denotes the average storm depth over an area A accumulated over a period of time Δt, and d_{min} is some minimum depth based on Δt and A, such that all storms having an effect on the exceedance probabilities are included in the sample.

In order to develop a complete SST model, we define the contents of a storm position vector $\mathbf{\Lambda}_p$ and a storm characteristics vector $\mathbf{\Lambda}_s$. The storm position vector $\mathbf{\Lambda}_p$ consists of storm center locations (x_s, y_s), defined as the location of the maximum observed total depth and are estimated from the extreme storm DAD database (Section 4.2). In this work, the storm position vector $\mathbf{\Lambda}_p$ is represented by a uniform probability distribution of storm centers in space, similar to previous investigators (Fontaine and Potter, 1989; Franchini et al., 1996). This relationship applies to a storm conceptualized with a single storm center (Hansen et al., 1982; England, 2006; England et al., 2007). It is modified for application to the Arkansas River watershed by limiting storm center locations (x_s, y_s) for larger-area storms within the basin. The stationary storm centers are located at lower elevations, with rainfall rates reduced at higher elevations within the mountainous watershed (Fig. 1), as discussed in Section 4.3. The storm characteristics vector $\mathbf{\Lambda}_s$ consists of the storm-total depth at 25.9 km^2 (10 mi^2) d_t, the total storm area A_s, the storm orientation θ and the storm major-to-minor axis ratio c. The d_t, A_s, θ, and c estimates in $\mathbf{\Lambda}_s$ are directly sampled from an extreme storm catalog (described in Section 4.2).

In addition to the storm position and characteristics vectors, spatial and temporal models of the storm rainfall are needed. In this study, an elliptical model for the spatial distribution of storm rainfall from Hansen et al. (1982) is used, with parameters c and θ (England et al., 2007). With this model, it is assumed that the storm is single-centered, and isohyets are geometrically similar in the form of an ellipse. This assumed storm shape describes both within-storm amounts and storm totals, and is an adequate spatial representation based on previous investigations of the DAD data (Foufoula-Georgiou and Wilson, 1990; England, 2006). The storm temporal model that describes the time-varying rainfall depth or rates over the storm duration is based on normalized mass curves (Huff, 1967; Koutsoyiannis and Foufoula-Georgiou, 1993) using DAD data (e.g., Franchini et al., 1996). Normalized mass curves are obtained using DAD data by: (1) dividing the cumulative storm depth d at time t by the total storm depth and (2) dividing the time t by the total storm time (Koutsoyiannis and Foufoula-Georgiou, 1993). Examples of these curves for two Colorado Front Range storms (May 1894 and June 1921) are shown in England (2006). Rain rates r [L/T] are determined by simple difference from each successive cumulative depth d.

4.2. Database of extreme storms

A new electronic database of extreme storms and pertinent characteristics was developed from existing data sets and supplemented by individual analysis of recent extreme storms. The data-

base was developed to provide quantitative estimates of extreme storm rainfall in space and time for estimating extreme storm probabilities and subsequent runoff modeling (Section 5). Three extreme storm data sources were used to develop the database. The first is depth-area duration (DAD) data from USACE (1973) and Bureau of Reclamation cooperative storm studies with the National Weather Service. These DAD data are used nearly exclusively in developing regionalized hydrometeorological reports that provide PMP estimates for this region (Hansen et al., 1988). The second source is an extreme storm catalog for Colorado from the Colorado Climate Center (CCC) for the period 1864–1996 (McKee and Doesken, 1997). The third source is individual extreme storm analyses and reports from the CCC completed after 1996, including the July 1997 Fort Collins (Doesken and McKee, 1998) and Pawnee Creek (Doesken, 1998) events.

A geographic region based on Hansen et al. (1988) was used to select storms from the database for consideration in developing extreme storm probability estimates. This large region covers the United States from Canada to Mexico, and between about longitude 99° and the Continental Divide. About 110 extreme storms with some DAD information are located in the region, and correspond to those used for PMP (Hansen et al., 1988). The storm database includes: DAD data with storm area A_s and various depths d_t for specific durations and area sizes; storm start and end dates; assignment number; total duration (t_s); maximum center location; latitude and longitude of storm center (x_s, y_s); storm period; and storm start and end times. The storm orientation θ and major-to-minor axis ratio c were estimated from the DAD summaries for each event.

An investigation of the storm database for the region indicates that there have been several extreme flood-producing rainstorms in the lower elevation portions of the Arkansas watershed. The largest flood-producing storms that have occurred within the Arkansas watershed are the May 1894 and June 1921 storms. Both of these events were used in rainfall–runoff model calibration (England et al., 2007). The majority of observed Colorado Front Range flood-producing storms are shorter duration (generally less than 24 h), high-intensity convective events (e.g., Follansbee and Sawyer, 1948). In some cases these are embedded in longer-duration storms that produce somewhat heavy rainfall over several days. Extreme rainfall within these convective storms is typically limited in areal extent, from tens to several hundreds of square kilometers. Based on the extreme storm catalog, there is a lack of evidence of longer duration, cyclonic storms that cause flooding in the Colorado Front Range at elevations higher than about 2300 m; this corroborates previous investigations of regional rainfall and streamflow records (Jarrett, 1987, 1993), paleoflood information (England et al., 2010) and radar-based storm analyses within the Arkansas watershed (Javier et al., 2007).

4.3. Application to the Arkansas River basin

The SST model is applied for the first time to the large, mountainous Arkansas River watershed; predictions are then used as input to the TREX rainfall–runoff model (Section 5). An analysis using results from storm-based radar studies (Javier et al., 2007) demonstrates storm center location and areal distribution effects on basin-average rainfall depth predictions. A storm transposition region A_{tr} for the Arkansas River basin was selected (Fig. 3) based on: (1) extreme storm catalog data; (2) storm type and topographic considerations; and (3) previous PMP and rainfall studies (Hansen et al., 1988; McKee and Doesken, 1997). The region encompasses the approximate 1,028,700 km^2 (397,200 mi^2) area between the Continental Divide (CD) and the 103rd meridian (CD-103). The basin orography and CD boundary play a major role in estimating the spatial distributions of extreme storm centers and storm areas within the region and the watershed, with many of the largest storms located in the foothills east of the CD. For storm simulations with SST and TREX rainfall–runoff modeling, the 11,869 km^2 watershed is discretized using a 960 m grid cell size (12,879 cells) to accurately capture storm center locations, storm spatial patterns, and channel geometry (England et al., 2007).

A subset of the extreme storm DAD data were used to implement the SST model and estimate extreme storm probabilities for the Arkansas River basin (England, 2006). The subset was utilized to ensure catalog completeness of extreme storms, and to ensure the inclusion of the largest extreme storms in estimating the upper tail of the distribution. The DAD catalog is incomplete, especially for moderate-intensity storms (NRC, 1988; Foufoula-Georgiou, 1989; Foufoula-Georgiou and Wilson, 1990). The criterion for the subset of storms to be included in the analysis and transposed, using Eq. (3), is:

$$\textit{Criterion } E: \quad \{\bar{d}[\Delta t = t_s,\ A = 25.9\ \text{km}^2] \geqslant 27.9\ \text{cm}\}, \tag{4}$$

which means that the extreme storm set is composed of storms that had a maximum observed 25.9 km^2 (10 mi^2) total depth over the whole storm duration t_s exceeding 27.9 cm (11 in). This magnitude/area criterion was chosen in order to ensure that the SST model is based on a complete extreme storm sample. Storm magnitudes less than 27.9 cm may not be recorded or included in the data base; the 25.9 km^2 area enabled examination and comparison with point rainfalls so that all extreme storms were included. Wilson (1989) and Foufoula-Georgiou (1989) used similar criteria for selecting and transposing storms in the Midwest. Fifteen extreme storms were selected based on this criterion; pertinent properties d_t, A_s, θ, and c are listed in Table 2. These are the most extreme storms within the region; nearly all were used to define PMP (Hansen et al., 1988), with the exception of the July 1997 event (subsequent to the PMP report). Storm rainfall depths ranged from 29.7 to 56.4 cm, and areal extents from 130 to 246,100 km^2.

The spatial occurrence of storm centers was assumed to be a homogeneous Poisson process. Given the limited number of storms used, and their geographic centers (Fig. 3), this means that storm transposition probabilities are equal within A_{tr}, and are independent of storm properties. A uniform spatial model for all depths was used, and $\mathbf{\Lambda}_p$ consists of (x, y) with uniform probabilities in space. This simplification was also made by Foufoula-Georgiou (1989) and Franchini et al. (1996), and is sufficient for providing initial estimates of basin-average rainfall depth probabilities for subsequent runoff modeling. The temporal occurrence model of extreme storms was simplified to a Bernoulli process with a success probability p_s and estimated by:

$$\hat{p}_s = \frac{N_s}{N}, \tag{5}$$

where N_s is the number of extreme storms, and N is the number of years of record. Based on the DAD storm data (Table 2), $\hat{p}_s$ is 0.144 with $N_s = 15$ and $N = 104$ years (1894–1997).

Stochastic storm transposition was applied using the actual storm properties ($\mathbf{\Lambda}_s$) for duration (d_t), areal extent (A_s), orientation (θ), and ellipse (c) parameters (Table 2). Spatial and temporal properties from each observed storm were used directly in Eq. (1). Annual probabilities $G^a(d)$ are determined as follows. First, the storm occurrence probability $\hat{p}_s$ is estimated. Second, the effective area $A_{eff,j}$ for storm j is estimated, as described below. Basin-average depths $\bar{d}_c(\Delta t) \geqslant d$ are estimated by simulating each observed storm j 1000 times uniformly within the effective area for that storm ($A_{eff,j}$) over the watershed. These depths vary in each simulation because we uniformly sample a storm center location (x_s, y_s) for each simulation. The probabilities $\hat{p}_j$ are determined for each storm by ranking by depth $\bar{d}_c$, then summed over all storms N_s.

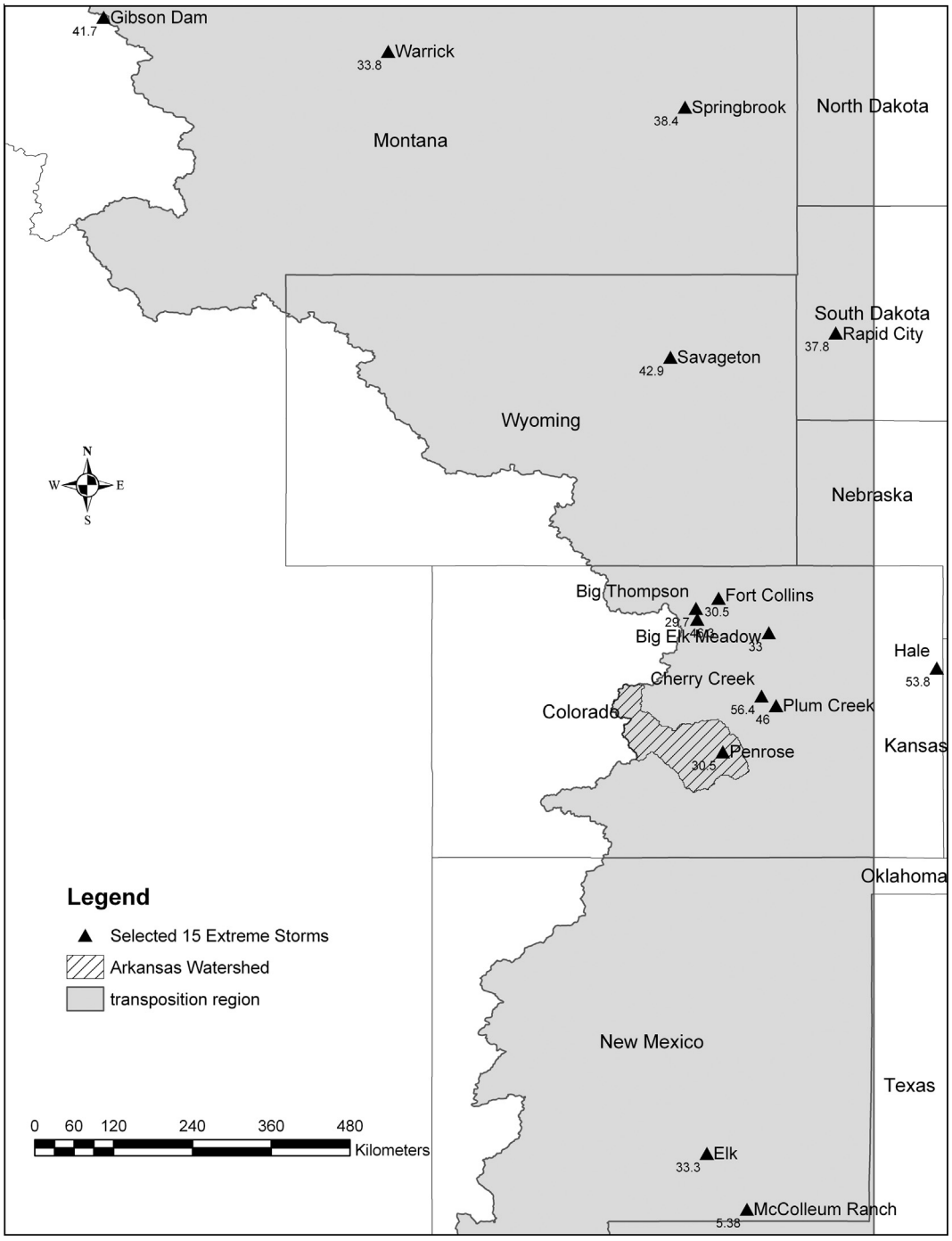

Fig. 3. Storm transposition region and spatial distribution of the 15 selected extreme storm centers. The black triangles show storm names and 25.9 km^2 storm total depth (cm); other storm properties are listed in Table 2. These are the largest extreme storms for the period 1894–1997, and their magnitudes have not yet been exceeded.

Here, a direct approach was developed to account for the actual basin geometry and interaction with each storm pattern to estimate $A_{eff\,j}$. Using the June 1921 storm as an example, the orientation, areal extent and ellipse parameter c dictate the interaction of the watershed and the storm (Fig. 4a). By placing the storm center (x, y) at every watershed cell, one obtains the storm-dependent effective area for the particular watershed of interest. This approach allows a direct way to account for partial area rainstorms over watersheds using SST, an effect that had not been previously implemented in prior SST applications. For example, Foufoula-Georgiou (1989) and Wilson and Foufoula-Georgiou (1990) used simple shapes (circles, ellipses, triangles and rectangles) for storms and watersheds, and were able to use analytical methods to estimate the watershed-storm interaction. The complex geometry of the Arkansas River watershed precludes these simpler approaches.

The approach to estimate $A_{eff\,j}$ was modified to enable limiting storm centers (x_s, y_s) based on location using spatial and causal information (e.g., Merz and Blöschl, 2008a). The flood runoff characteristics indicate that the transition zone between rainfall–runoff and snowmelt runoff is near Parkdale (England et al., 2010). Within the Arkansas watershed, the largest observed extreme storms (Fig. 3) and recent storm analyses based on radar (Figs. 9 and 12 in Javier et al. (2007)) indicate that storm centers are located near the watershed outlet, initiated principally near Pikes Peak and the

Table 2
Fifteen extreme storms from the DAD catalog that are transposed to the Arkansas Watershed.

Date	Assignment No.	Location	State	Duration (t_s) (h)	Orientation (θ) (°)	Total 25.9 km^2 depth (d_t) (cm)	Max 24 h 25.9 km^2 depth (cm)	Areal extent (A_s) (km^2)	Ellipse (c)
05/30/1935	MR 3-28A	Cherry Creek	CO	24	47	56.4	56.4	16,300	4
09/20/1941	GM 5-19	McColleum Ranch	NM	78	16	53.8	30.7	98,400	3.5
05/30/1935	MR 3-28AZA	Hale	CO	24	32	53.8	53.8	3340	2
05/04/1969	19690504	Big Elk Meadow	CO	96	14	46.3	30.0	13,000	2
06/13/1965	SW 3-23	Plum Creek	CO	181	5	46.0	33.5	101,700	1.5
09/27/1923	MR 4-23	Savageton	WY	108	46	42.9	24.1	246,100	2.5
06/06/1964	NP 2-23	Gibson Dam	MT	36	141	41.7	37.8	31,300	2
06/17/1921	MR 4-21	Springbrook	MT	108	38	38.4	33.8	136,200	1
06/09/1972	MR 10-12	Rapid City	SD	12	172	37.8	37.8	5180	2
06/06/1906	MR 5-13	Warrick	MT	54	90	33.8	25.9	103,600	1.2
07/21/1905	GM 3-13	Elk	NM	108	80	33.3	14.5	114,000	1.5
06/12/1949	R7-2-5	Prospect Valley	CO	36	63	33.0	23.1	930	2
06/02/1921	SW 1-23	Penrose	CO	114	0	30.5	30.5	2590	2.5
07/27/1997	19970727	Fort Collins	CO	32	0	30.5	25.4	2590	2
07/31/1976	19760731	Big Thompson	CO	4	25	29.7	29.7	130	3.5

Wet Mountains (Fig. 1). Based on the flood hydrology, distribution of extreme storm center locations with elevation, and storm radar investigations, extreme storm centers are restricted to locations east of Parkdale. This results in a reduction of $A_{eff\,j}$, as shown for the June 1921 storm in Fig. 4b. Data and analyses also suggest that there are restrictions to the size of extreme storms that occur in the Arkansas watershed. Core rainfall areas within the most extreme storms that have occurred immediately adjacent to the foothills, such as the June 1921 Penrose storm (England et al., 2007), the July 1976 Big Thompson storm and the July 1997 Fort Collins storm, occurred over areal extents less than 12,950 km^2, and at lower elevations along the foothills east of the CD (Figs. 2 and 3).

4.4. Basin-average rainfall depth probabilities

Basin-average depth probabilities are estimated using Eq. (1) and the data from the 15 extreme storms (Table 2). Two cases are used to illustrate the major SST factors and variations in basin-average precipitation frequency distributions: (1) unrestricted storm centers and areas; and (2) storm center and area restrictions based on data and process considerations. The results of the simulations are shown in Fig. 5, with effective storm area estimates in Table 3. The shape of the basin-average depth distribution (unrestricted case) is generally similar to that obtained for smaller 2590 km^2 (Foufoula-Georgiou, 1989) and 5180 km^2 (Wilson, 1989) hypothetical circular watersheds in the Midwest. The upper tail of the distribution is also similar in shape to other SST analyses in the Midwest (Fontaine and Potter, 1989; Wilson and Foufoula-Georgiou, 1990). This upper tail shape is driven by the extreme storm data utilized, the use of fixed storm parameters, and interactions of the storms with the watershed. The shapes and magnitudes are insensitive to the inclusion of five additional extreme storms, and increasing the number of simulations of each storm (j in $A_{eff\,j}$) from 1000 to 10,000 (England, 2006). The depth distribution includes the AEPs of interest (0.001–0.00002) for risk analysis (noted in Section 2), and encompasses the design basin average rainfall estimate for Pueblo Dam (26.72 cm in 27 h over 5180 mi^2), but is less than the PMP general storm basin average depth estimate (34.8 cm in 72 h over 12,137 km^2). This large difference suggests that runoff from the PMP may substantially overestimate flood magnitudes used for dam safety analysis for this watershed.

The probability distribution of storm depths was estimated considering storm center and area restrictions based on data and process considerations. Storm centers were restricted to locations east of Parkdale, and represent what is observed from radar (Javier et al., 2007) (Fig. 4b) and regional extreme storms. The maximum storm area was restricted to 12,950 km^2 to reflect lower-elevation, orograpically-enhanced storms near the lower portion of the watershed (Fig. 1), and radar considerations. Results of the storm center and area restriction simulations are shown in Fig. 5. Effective area estimates for these cases are listed in Table 3. The restriction of storm centers east of Parkdale and areas results in a shifted frequency distribution to smaller exceedance probabilities, due to a reduction of A_{eff} by about a factor of 2–5 (Table 3). The extreme tail of the distribution also drops more quickly, and estimated maximum depths are lower by about 20%. The shape of the upper tail for this case is similar to the unrestricted case. Clearly, storm center locations and storm areas are critical factors in basin-average rainfall frequency distributions. England (2006) examined basin-average SST sensitivity for other factors, including number of extreme storms considered, number of simulations, and additional center and area restrictions, with results similar to those shown in Fig. 5. Secondary features, such as storm tracking and movement, could be considered as part of future work, compared to these factors. In our case, the watershed is at partial-equilibrium and stationary rainstorms typically result in higher peaks. The effect of tracking was approximated by selecting storm center locations (east of Parkdale) based on hydrometeorological insights. Storm movement might be particularly important for highly-convective rainfalls at smaller storm area and watershed scales. Such considerations might be important for local flash floods, but are less important for watershed analyses at the spatial scale of the Arkansas River basin. As this framework focuses on larger watersheds, one primary driver is the extreme storm duration with most storms exceeding 24 h, rather than storm movement.

5. Flood frequency with a distributed model

The Two-dimensional, Runoff, Erosion and Export (TREX) model (Velleux et al., 2006, 2008, 2011; England et al., 2007) is used to estimate flood runoff hydrographs from extreme storm rainfall over the Arkansas River basin. We briefly describe this physically-based model, then present the use of TREX to estimate extreme flood probabilities and investigate model performance with independent paleoflood data at an internal watershed location and the outlet.

5.1. TREX model overview

TREX is a fully-distributed and physically-based watershed model that simulates rainfall–runoff, sediment transport, and

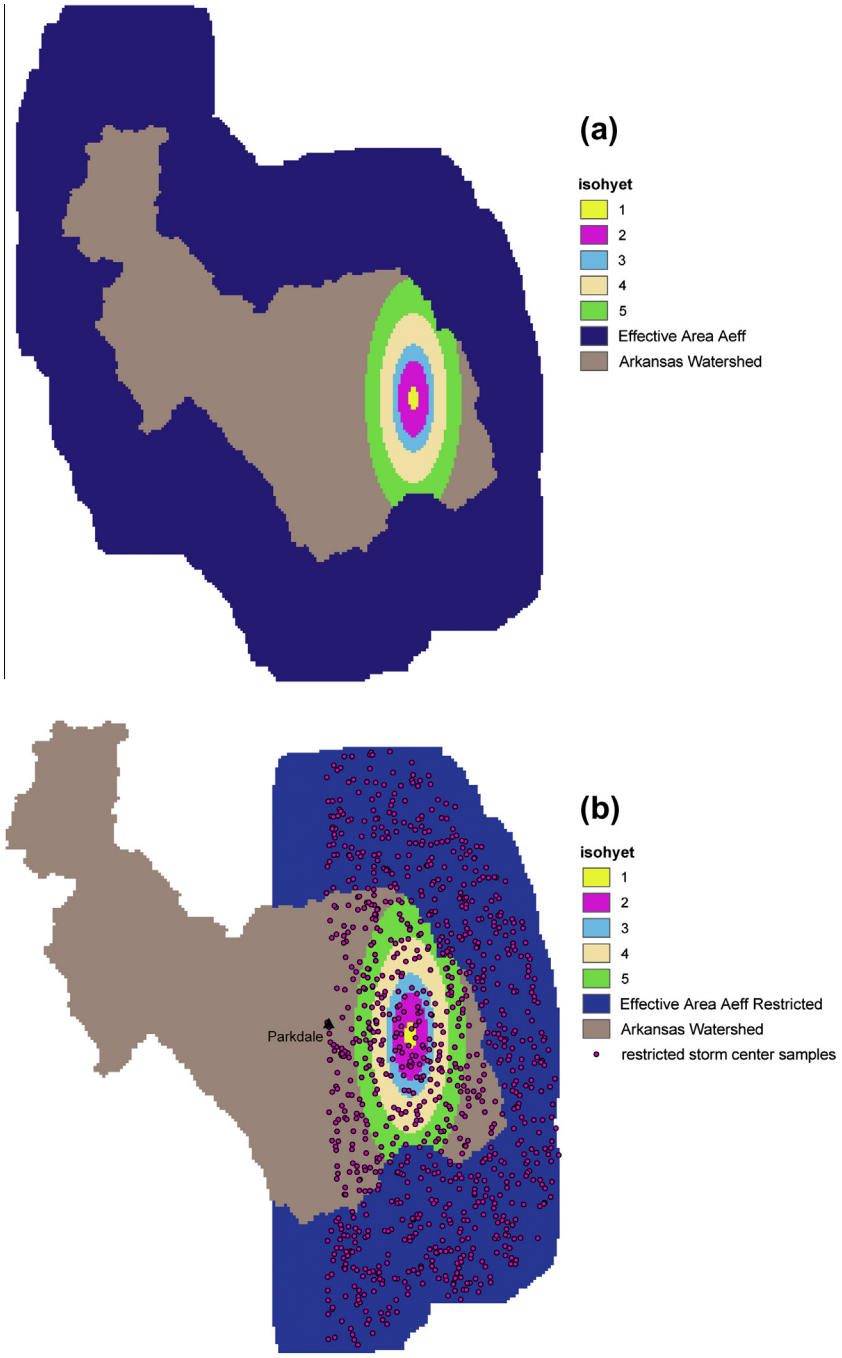

Fig. 4. Stochastic storm transposition example effective storm area A_{eff} determination for the June 1921 storm over the Arkansas watershed. A_{eff} based on uniform storm centers over the watershed is show in (a). A_{eff} based on limiting storm centers west of Parkdale is shown in (b); red dots indicate positions of 1000 simulated storm centers. By utilizing the flood and storm characteristics to limit storm centers, there is a dramatic reduction in A_{eff}; results for the 15 storms are listed in Table 3.

chemical fate and transport for individual events. In this work, we utilize key hydrological components for a semi-arid watershed that include: 2D diffusive wave, overland (Hortonian) flow; 1D diffusive-wave river channel flow with spatially-varying widths and depths; spatially-varied rainfall using depth-area-duration (DAD) data and an elliptical storm pattern (Section 4); and Green–Ampt infiltration. Within TREX, processes are implemented on a regular grid (Velleux et al., 2008). This spatially-explicit approach directly accounts for partial-area rainfalls, variation in storm center locations, and spatial channel properties derived from field measurements (England et al., 2007). On large watersheds, key flood processes (spatial distribution of rainfall and travel time in channels) that can significantly affect the flood frequency curve are directly modeled with TREX. Using TREX for the runoff modeling portion of the framework is attractive and appropriate with diffusive-wave routing (2D overland, 1D channels), because the watershed geometry of hillslopes and channels is directly preserved, capturing the spatial distribution of storms, the storm locations, and overland flow and channel hydrodynamics directly. The routing scheme is particularly attractive and appropriate for large watersheds (Ponce, 1989), rather than simpler routing schemes previously used in flood frequency (Table 1), because it can affect peak-flow response. There are additional research opportunities to explore the use of fully-distributed,

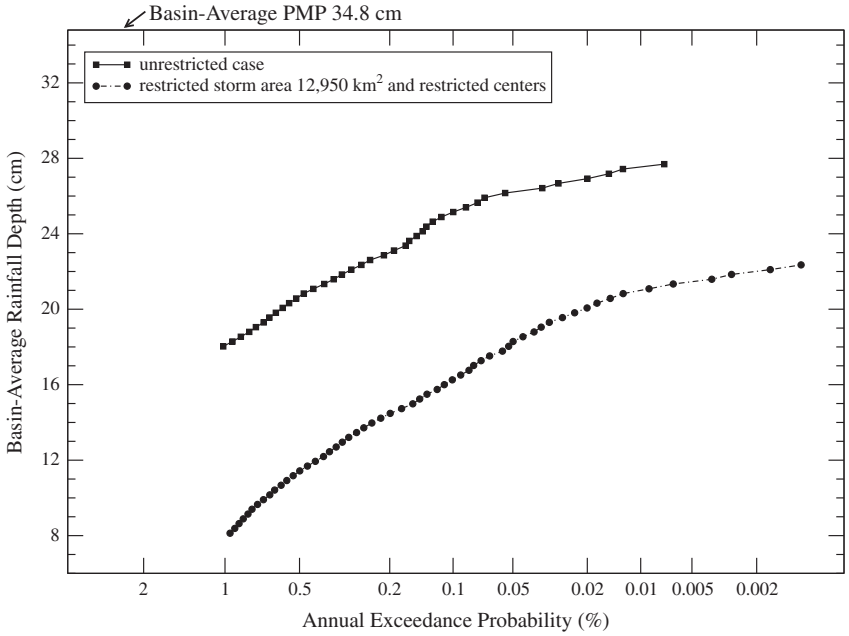

Fig. 5. Arkansas River watershed basin-average rainfall depth (d_c) annual exceedance probabilities for two cases: an unrestricted case; and restricting storm center locations and storm areas. The difference between these two cases is the effective area (A_{eff}) for each storm is reduced by limiting storm centers and areas (Table 3). Refer to the text for additional details.

Table 3
Storm-watershed interaction effective area estimates for unrestricted case and restricted storm centers and storm areas.

Assignment No.	Simulated storms (unrestricted case)		Restricted storm centers west of Parkdale and storm areas limited to 12,950 km^2	
	Aeff (km^2)	Aeff/Atr	Aeff (km^2)	Aeff/Atr
MR 3-28A	105,590	0.103	47,830	0.046
MR 3-28AZA	40,460	0.039	18,220	0.018
GM 5-19	286,010	0.278	44,390	0.043
19690504	73,810	0.072	39,850	0.039
SW 3-23	219,300	0.213	34,110	0.033
MR 4-23	537,100	0.522	40,060	0.039
NP 2-23	106,270	0.103	37,180	0.036
MR 4-21	210,590	0.205	25,880	0.025
MR 10-12	45,050	0.044	22,840	0.022
MR 5-13	189,740	0.184	26,820	0.026
GM 3-13	240,500	0.234	30,260	0.029
R7-2-5	25,680	0.025	10,280	0.010
SW 1-23	36,040	0.035	16,530	0.016
19970727	36,040	0.035	16,530	0.016
19760731	16,620	0.016	6,390	0.006

hydrodynamic watershed models of this class for hydrologic hazard applications. This framework is also a way to eventually explore the non-linear, physical features in the flood frequency curve.

The main hydrology-related parameters used in this Arkansas River extreme flood application include: Manning n for overland and channel flows; and Green–Ampt parameters for effective porosity θ_e, effective suction head ψ, saturated hydraulic conductivity K_S and effective soil saturation S_e. Initial soil moisture is expressed using a saturation fraction S_e (Velleux et al., 2008). The infiltration and overland flow parameters are regularized based on soils (18 classes) and land-use (9 classes) grids, respectively (England et al., 2007). The TREX model has been previously applied to the Arkansas River basin, in order to simulate the record June 1921 flood, a May 1894 flood, and runoff from the Probable Maximum Precipitation (England et al., 2007). A 960 m grid cell size is used for runoff modeling, with 764 channel cells. The channel network (Fig. 6, dark line) includes the Arkansas River and all main tributaries in this bedrock-controlled, deep canyon environment. A constant time step equal to 2.5 or 5 s is used, depending on rainfall inputs, for computational stability. We utilize model parameter estimates and inputs for flood frequency based on these previous calibration and validation efforts. Full details on watershed input geometric data (including surveyed channel cross sections), and model parameter estimates are provided in England (2006) and England et al. (2007). This is the first use of the TREX model to estimate an extreme flood frequency curve. Model estimates from TREX are subsequently compared to flood frequency curves based on paleoflood data.

5.2. Flood frequency estimates with extreme storms

In order to estimate a flood frequency curve, the rainfall inputs to the TREX model were those storms used in stochastic storm transposition (Table 2). Basin-average depths were selected for specified AEPs in the general range of 0.01–0.0001 (100-year to

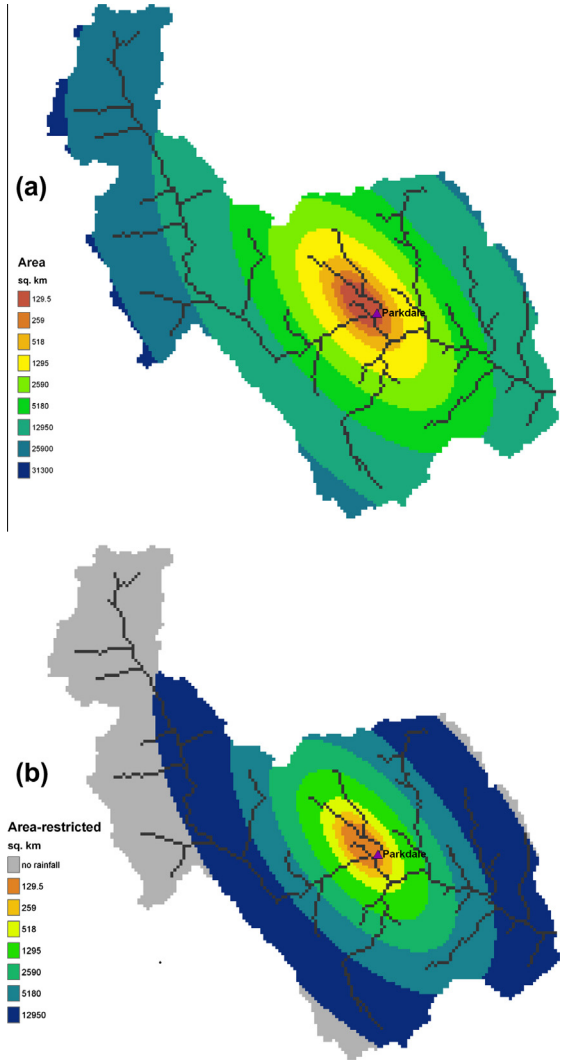

Fig. 6. Storm spatial pattern for TREX model runs and flood frequency: (a) storm rainfall area (31,300 km^2) over watershed; (b) restricted storm area (12,950 km^2) over watershed based on radar data, storm catalog, and flood runoff mechanisms. River channel network shown as dark lines.

10,000-year storms), from basin-average rainfall frequency curves (Fig. 5). Storms were then constructed to distribute the basin-average rainfall depths in space and time over the watershed using an actual storm as input to TREX. The following storm properties are initially considered fixed: storm center location, orientation, storm area, ellipse parameter, spatial and temporal distributions. The storm center locations and areas are subsequently modified to reflect storm data and process considerations. The storm that contributed the largest depths in the SST (Gibson Dam, NP2-23, June 1964, Fig. 3) was selected as the base pattern. This storm covers 31,300 km^2, has an orientation of 141°, c = 2.0 and the duration is 36 h (Table 2). This storm was transposed to Parkdale, and the storm spatial distribution covers the entire Arkansas River watershed (Fig. 6a). The orientation most likely optimizes flood runoff production, as the major axis is nearly in line with the river in the lower watershed. A restricted storm area utilizes the same storm center and orientation pattern (Fig. 6b).

The input to the TREX model for flood frequency consisted of the storm with area amounts adjusted to meet the target basin-average depth, and the calibrated model parameters. The initial soil saturation S_e was set to 0.5 for each run. This median estimate is based on the two largest events in the watershed (England et al., 2007); S_e sensitivity is shown in Section 5.4. The flood frequency curve was then estimated by selecting rainfall depths from the basin-average rainfall frequency curve and running the model for each specified depth. The peak-flow probabilities are approximate (e.g., NRC, 1988), as the runoff model inputs are held constant except for the rainfall depth, which is the dominant factor that contributes to the peak flow distribution. The complete rainfall depth frequency curve is discretized into sixteen points for subsequent runoff modeling. The TREX model is computationally intensive; computer time to complete 16 model runs for the rainfall depths ranged from five to 16 h, depending on model inputs.

The resulting TREX flood frequency curves at four key points within the watershed (locations in Fig. 1) are shown in Fig. 7. The peak-flow frequency curves shown are approximate, because the results reflect rainfall depth probabilities, median S_e conditions, and best estimate (average) soil and channel parameters, that are AEP-neutral (e.g., Nathan and Weinmann, 1999). Additional research on the SST model, TREX model parameters, and TREX computational efficiency for Monte-Carlo simulations is needed, in order to estimate frequency curves based on sampling input storm and model parameter distributions. Additional research to provide uncertainty estimates would also be valuable. The flood frequency curve at Pueblo has the same overall shape as the rainfall frequency curve (Fig. 5). The main portion of each distribution from 1 to 0.1 percent is nearly Normally distributed; the tails of the rainfall and peak-flow distributions then flatten. Clearly, the rainfall distribution upper tail affects the shape of the peak-flow frequency curve similar to GRADEX (e.g., Naghettini et al., 1996). Flood frequency curves at Salida, Wellsville, Parkdale and Pueblo show the dramatic reduction in peak flow magnitude from downstream rainfall–runoff sites to upstream snowmelt sites as observed with field measurements. The spatial rainfall distribution and storm center location are the principal factors in the relatively dramatic reduction of peak flows from downstream to upstream sites. Spatial distributions of rainfall and runoff depth over the watershed at the initiation of large main channel depths (Fig. 8a) and at peak runoff discharge (Fig. 8b) demonstrate these controlling factors on peak flow (see water depth animation in Supplemental material). Runoff hydrographs for the largest simulated rainfall depth (basin average 27.7 cm), that has an estimated AEP of 0.00007, are shown in Fig. 9. The hydrograph shapes indicate that the TREX model is stable and can simulate extreme floods on watersheds of this scale. The hydrographs also reflect the spatial distribution of storm rainfall; flows are substantially larger over the lower, downstream portion of the watershed (Parkdale and Pueblo).

The effects of varying storm center locations and storm areas on TREX model peak-flow predictions is examined. Storm centers are restricted to locations east of Parkdale and storm areas are restricted to 12,950 km^2. A rainfall frequency curve for this case is shown in Fig. 5. A peak-flow frequency curve estimated using TREX for this case is shown in Fig. 10. Effective storm area ratios (A_{eff}; Table 3) provide insight into the changes in these frequency curves. The restriction in the storm spatial distribution (center and area) significantly affects the peak-flow frequency curve shape. As the storm location within the watershed is restricted, and storm areas reduced, the peak flow frequency curve shifts to the right so that a given peak discharge is less frequent. The reduction in effective storm area (Table 3) causes a reduction in peak-flow probabilities; the tails of the distributions are extended (Fig. 10). The frequency curve for restricting storm areas steepens because for a fixed basin-average rainfall, the depth is distributed over a smaller area. The outer two ellipses of the storm pattern as shown in Fig. 6a are eliminated (see Fig. 6b and water depth animation in Supplemental material). These peak-flow frequency curves mimic the shapes of the rainfall frequency curves (Fig. 5).

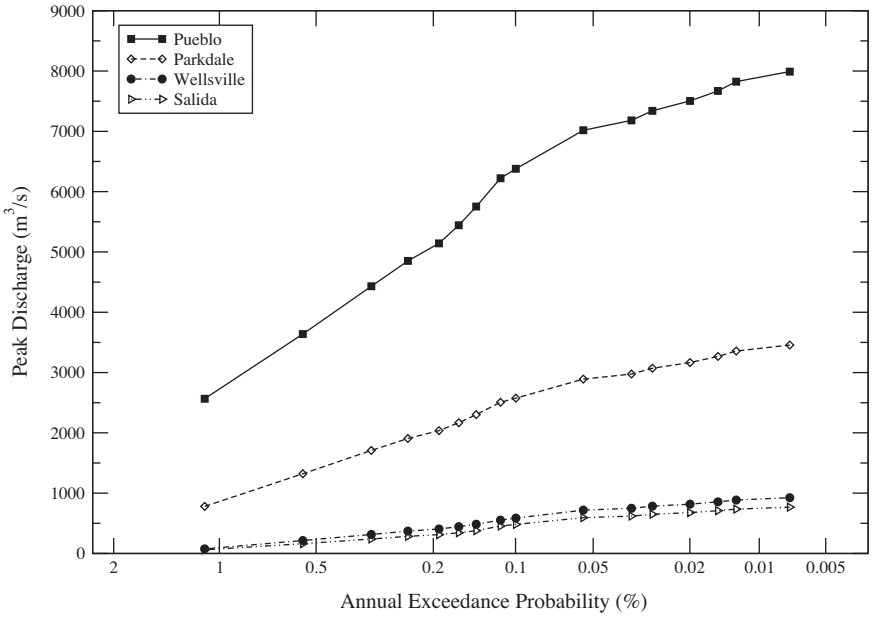

Fig. 7. Flood frequency curves at Pueblo, Parkdale, Wellsville (Loma Linda) and Salida (Adobe Park), estimated from TREX simulations (unrestricted rainfall case). Flood magnitude is dramatically less for upper basin sites (Wellsville and Salida) compared to lower basin sites, because of much lower rainfall rates.

5.3. Paleoflood data comparisons

One of the largest and most devastating floods in Colorado occurred within the Arkansas River watershed at Pueblo on 3–4 June 1921 (Follansbee and Jones, 1922). England et al. (2010) describe paleoflood nonexceedance bound data that place this record flood event in a longer, 730–800-year time context, and provide data-based peak-flow frequency curves which are used as a basis to judge rainfall–runoff model predictions.

Paleoflood data and flood frequency estimates are available at four sites within the Arkansas River basin: Adobe Park, Loma Linda, Parkdale and Pueblo State Park (Fig. 1). Runoff mechanisms within the Arkansas watershed were distinguished between snowmelt (Salida and Wellsville) and rainfall–runoff (Parkdale and Pueblo). The focus of these comparisons is thus in the lower watershed at Parkdale and Pueblo as we simulate runoff from extreme rainfalls with TREX. The TREX model flood frequency curves at the two downstream, rainfall–runoff dominated locations (Pueblo and Parkdale) are compared with peak-flow frequency curves based on streamflow, historical and paleoflood data using the LP3 distribution and EMA (Cohn et al., 1997) with data and frequency curves presented in England et al. (2010). Here we are interested in the differences in flood frequency shapes, how the TREX model-generated frequency curves compare with the LP3 curves, if they fall within the confidence intervals, and if they match magnitudes and plotting position estimates (Hirsch and Stedinger, 1987) of the largest floods and paleoflood nonexceedance bound data. The basic concept for making the comparisons is that the TREX model flood frequency curve should be "consistent" with the gage, historical and paleoflood peak flow estimates.

The TREX model flood frequency curves and LP3-EMA paleoflood frequency curves at Pueblo and Parkdale are shown in Fig. 11a and b. Paleoflood nonexceedance bound data for each site are listed in boxes within each figure. There are about 790 years of information at Pueblo and about 1200 years at Parkdale. Data and LP3-based frequency curves are extrapolations beyond about 0.001 AEP; LP3 EMA confidence intervals (Cohn et al., 2001; England et al., 2010) reflect this record length. TREX results based on the SST rainfall distributions (Fig. 5) are shown; we address each of these results in turn.

The first comparisons are TREX results at Pueblo and Parkdale based on the SST unrestricted rainfall case (total storm over watershed), shown as dashed lines with filled blue squares. Clearly, TREX flood frequency curves are larger than the data-based frequency curves at both locations. At Pueblo (Fig. 11a), the TREX results exceed both the largest flood observation (June 1921) and the paleoflood nonexceedance bound by about 1.7. TREX results are about 3 times larger than both the largest flood and paleoflood nonexceedance bound at Parkdale (Fig. 11b). The lower portion of the curve at Pueblo, as well as the entire curve at Parkdale, appears too high compared to the data. This suggests that the rainfall magnitudes and potentially the initial soil moisture (Section 5.4) are too high; these factors are subsequently varied. Interestingly, the extreme upper tail of the TREX frequency curve at Pueblo is within the data-based upper 95% confidence limit. This upper tail is directly related to the rainfall distribution. The shapes of the TREX flood frequency curves are also distinctly different than the positive-skewed, data-based LP3 distributions. They have flatter slopes in the main portion of each curve and relatively flat tails, also due primarily to the rainfall distribution (Fig. 5).

Now we examine TREX flood frequency predictions compared to data, considering the SST rainfall case restricting storm locations east of Parkdale and storm area less than 12,950 km^2. The basin-average rainfall frequency curve for this case is shown with filled circles in Fig. 5, with the restricted storm rainfall spatial pattern (Fig. 6b). As noted in Section 4.4, this case best represents actual extreme storm center initiation locations and storm area sizes. TREX flood frequency results are shown as red solid lines with diamonds at Pueblo (Fig. 11a) and Parkdale (Fig. 11b). The TREX model frequency curves at both locations changed fairly substantially from the unrestricted rainfall case; they have shifted downward in magnitude and have steeper slopes near the largest peak-flow observations (see also Fig. 10 at Pueblo). Results are also much closer to the largest observations. Importantly, the curve at Pueblo is consistent with the paleoflood nonexceedance bound data and well within the LP3 confidence interval, but the shape has a strong negative skew with a very flat upper tail (Fig. 11a), primarily due to the rainfall distribution, and perhaps channel routing effects. The TREX curve at Parkdale is close to the data in the lower tail, but still appears to be much higher than the data in the upper tail and

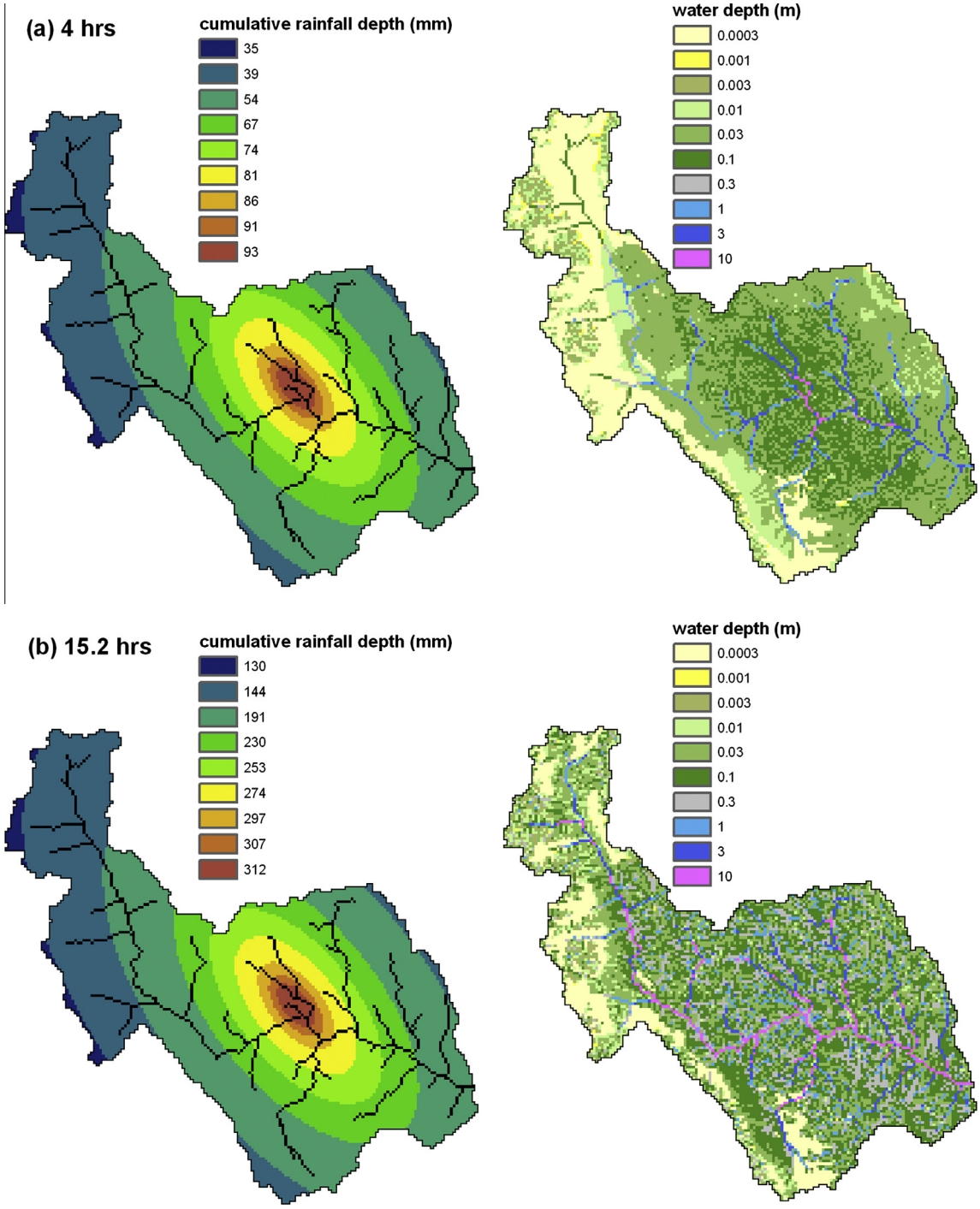

Fig. 8. Spatial distributions of cumulative rainfall and runoff (water surface depths) from the TREX model for the largest simulated flood event (unrestricted rainfall case): (a) initial large channel flows near storm center location (4 h) and (b) at watershed outlet peak (15.2 h).

inconsistent with the paleoflood nonexceedance bound. These two curves have different shapes than the data-based curves clearly because of the rainfall frequency distribution. As this rainfall distribution is based on stochastic storm transposition, there is no reason why the model and data-based LP3 flood distributions should necessarily be the same, as storms transposed into the watershed are not part of the observed flood records. At Pueblo, the data-based flood frequency curve is based partially on the June 1921 and May 1894 storms; these events were used in calibration/validation (England et al., 2007). The comparisons suggest that storms should be further limited in areal distribution, location, and/or intensity to reduce the peaks at Parkdale.

5.4. Initial soil moisture sensitivity

Initial soil moisture conditions play an important role in runoff predictions, and can affect infiltration rate, peak and volume, especially for event models such as TREX (e.g., Woolhiser et al., 1996; Viglione et al., 2009). The role of initial soil moisture in TREX peak-flow predictions is explored by varying the initial soil satura-

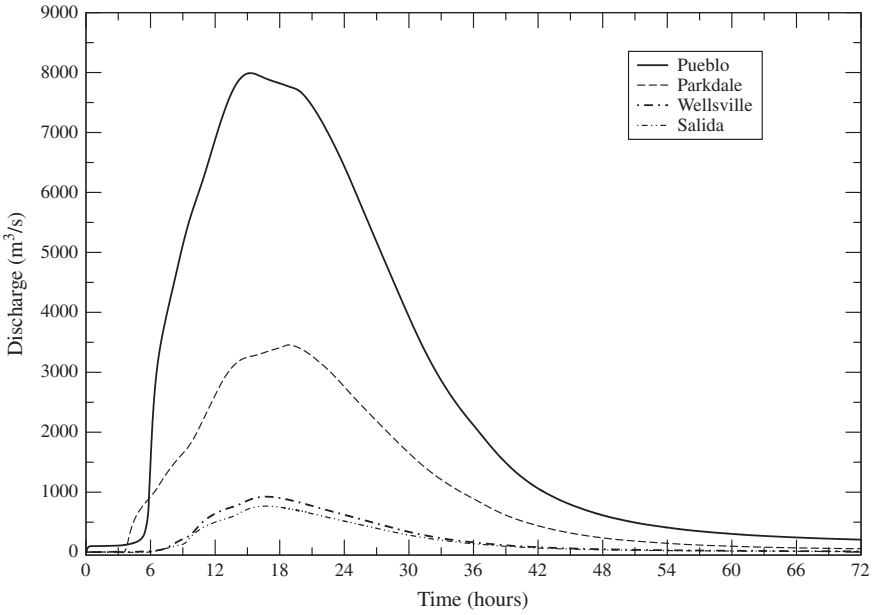

Fig. 9. Flood runoff hydrographs at Pueblo, Parkdale, Wellsville and Salida for the largest simulated rainfall depth (27.7 cm) over the Arkansas watershed (unrestricted rainfall case).

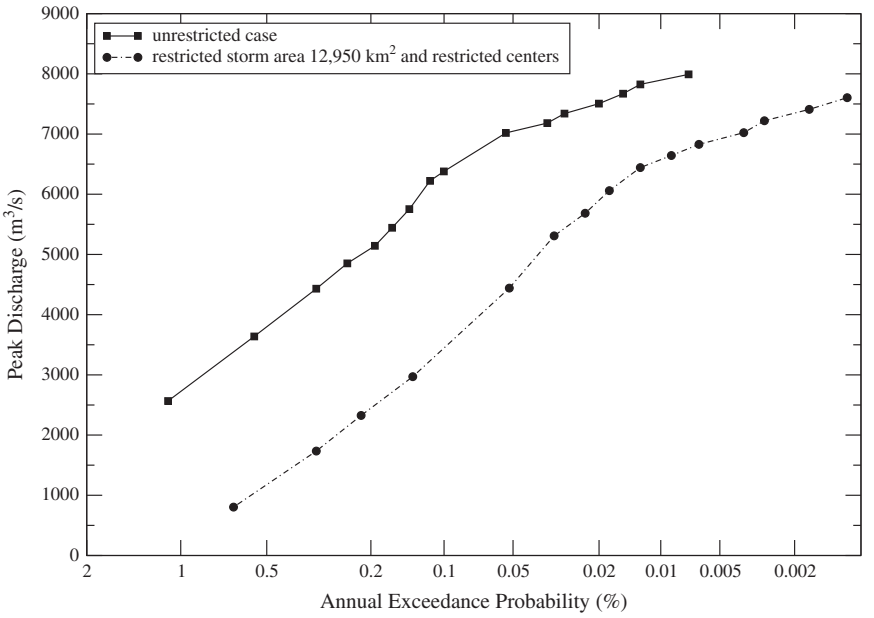

Fig. 10. TREX model flood frequency curves at Pueblo, showing effects of varying basin-average depth rainfall frequency for an unrestricted case and restricting storm center locations and storm areas.

tion S_e. The value used for the results shown above is 0.5, and represents a 50% saturation level across the watershed. Three saturation levels are chosen for sensitivity: 0.05 (dry), 0.2 (slight saturation) and 0.8 (near saturation). The initial soil moisture amounts were assumed to be uniform in space across the watershed domain, because detailed spatial information on soil moisture within the watershed is lacking.

The soil moisture sensitivity results are shown in Fig. 12 for the three sensitivity cases as compared to the $S_e = 0.5$ base case. In all runs, the location and area-restricted SST basin-average rainfall curve was used, and all other parameters were held constant. It is apparent that the soil saturation has a moderate effect on the predictions. The curves are shifted from the base run (shown with filled squares), but the frequency curves do not substantially change shape. The peak discharges and volumes (not shown) can increase by a factor of 1.20–1.75 for $S_e = 0.5$–0.8, or decrease by about 1.18–1.82 for $S_e = 0.5$–0.2. As rainfall (peak discharge) increases, the change in initial soil moisture has less of an effect; larger percent differences are observed for the lower peaks. The slope of the curves change slightly. The amount of change for the largest floods with $S_e = 0.8$–0.05 is 1.59, and for the more frequent floods the ratio with $S_e = 0.8$–0.05 is 2.52. Thus, the initial soil moisture

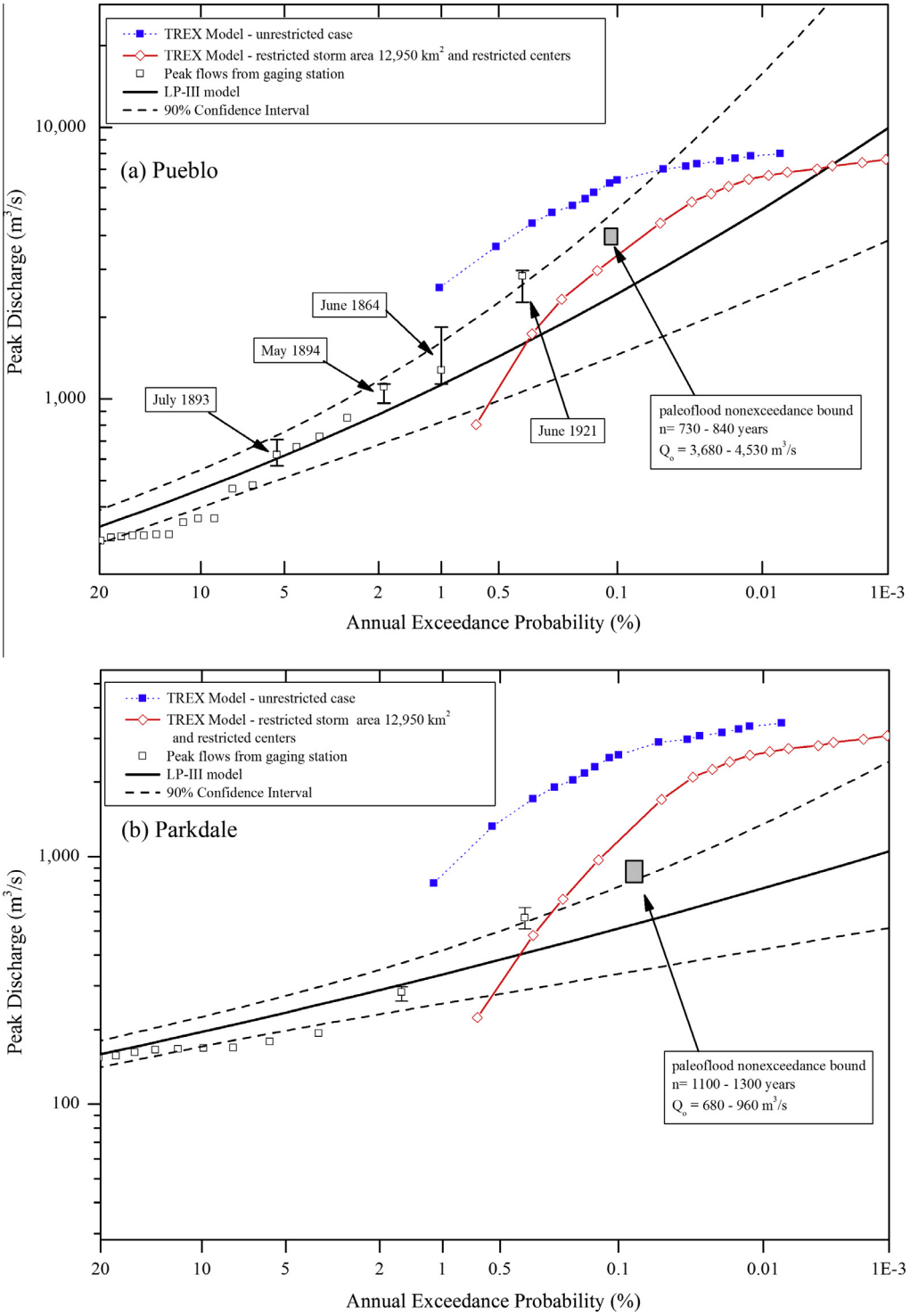

Fig. 11. TREX model flood frequency and streamflow/paleoflood frequency curves at rainfall-dominant sites (a) Pueblo and (b) Parkdale. Dashed lines with filled squares (blue) are TREX results based on SST unrestricted case (total storm over watershed). Solid lines with diamonds (red) are TREX results based on SST curve with restricted 12,950 km^2 storm area and restricted storm centers east of Parkdale. Peak-flow estimates from gage are shown as open black squares. Paleoflood nonexceedance bound data are shown as filled gray rectangles. (For interpretation of the references to color in this figure legend, the reader is referred to the web version of this article.)

does play an important role in flood peak predictions from TREX, depending on magnitude.

6. Summary and conclusions

An integrated data-modeling hydrologic hazard framework for physically-based extreme flood hazard estimation was presented to fully integrate hydrometeorology, flood hydrology and paleoflood hydrology. Key elements included: rainfall inputs from stochastic storm transposition, physically-based rainfall–runoff simulation with the TREX model, and independent streamflow and paleoflood data with peak-flow frequency curves at internal watershed locations. This approach was shown to integrate temporal (extreme storms, paleoflood and historical data), spatial

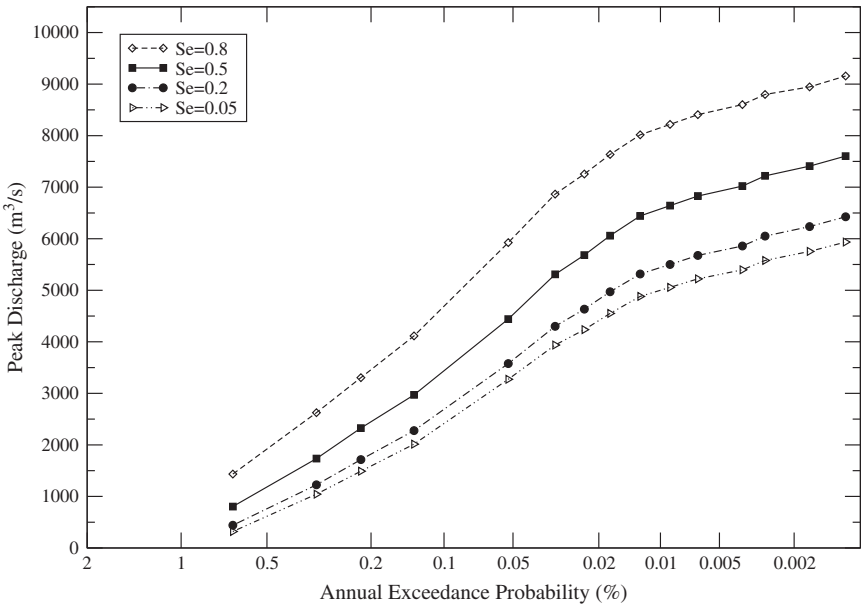

Fig. 12. TREX model flood frequency curves at Pueblo with varying initial soil saturation S_e (unrestricted rainfall case).

(extreme regional storms, spatial models conditioned by radar), and causal (flash floods, partial area, paleoflood) information. The TREX model with stochastic storm transposition (SST) was applied to the 12,000 km^2 Arkansas River basin, to estimate flood frequency curves. The study objectives were to: (1) implement and demonstrate the use of stochastic storm transposition on a large, orographic watershed; (2) utilize the TREX physically-based, distributed runoff model with SST rainfall to estimate extreme flood frequency (AEP $\leqslant$ 1/10,000); and (3) vary spatial rainfall and compare TREX predictions to streamflow and paleoflood data at internal watershed locations.

The TREX model with stochastic storm transposition provides a unique physically-based method for estimating flood frequency curves with space–time variability of rainfall and watershed characteristics and storm center locations. TREX model flood frequency estimates can be improved by using independent paleoflood data with peak-flow frequency curves within the watershed. Specific conclusions from the work are as follows.

1. A stochastic storm transposition model was developed and applied to the Arkansas River basin. The model directly accounts for storm-watershed interactions, partial area rainfalls, and actual watershed geometry. An extreme storm DAD database was developed and used to implement the SST model with data from 15 of the most extreme storms in a large region. Basin-average depths were less than the PMP for the watershed. Storm center locations and storm areas were shown to be critical factors in estimating effective rainfall area and basin-average rainfall distributions. The SST model thus exploited spatial information from radar and causal (elevation and flash flood versus snowmelt) within the watershed.
2. Using extreme flood probability concepts (NRC, 1988), the physically-based TREX model was coupled with SST to estimate extreme flood frequency curves. TREX peak flows at Pueblo for AEP 0.01–0.0001 were from 2550 to 8000 m^3/s for storms covering the entire watershed. TREX model frequency curves were generally higher than peak flow and paleoflood data-based frequency curves. Model upper tails were relatively flat compared to LP3 shapes, and were dominated by basin-average rainfall distribution shapes and magnitudes. Flood volumes and hydrographs from TREX (for each peak flow) can subsequently be used for hydrologic risk analysis.
3. The effects of storm location, storm area (basin-average rainfall distributions), and initial soil moisture on flood frequency predictions were illustrated. Flood frequency curves generally had very similar shapes to the rainfall frequency curves. A restriction on storm centers and areas reduced the peak flows and AEPs of the flood frequency curve. TREX model frequency curves at the two downstream flash-flood sites within the watershed were compared with data-based peak-flow frequency curves with paleoflood data. When restricting storm area and storm center locations at the outlet, the TREX frequency curve was consistent with the paleoflood nonexceedance bound data. Initial soil moisture, encompassing the potential range for extreme floods, can affect peak flows by a factor of 1.18–2.52 for the four cases considered (dry to near saturation).

There are several areas in which future research could be conducted to gain increased understanding of extreme floods and probability estimates within large watersheds such as the Arkansas River. The SST model implemented as part of this study could be improved in several areas, such as by estimating full distributions on storm center locations, storm depth-area relations, and temporal distributions, and developing procedures to estimate uncertainty of the rainfall depths. Additional extreme storm data collection efforts (e.g., England et al., 2008) would be needed to improve the SST rainfall model. Advances in understanding and estimating orographically-enhanced rainfalls, elevation effects, and their spatial patterns (e.g., Mahoney et al., 2012) are also needed. The feasibility of conducting full Monte-Carlo flood simulations with TREX could also be an area of future research, but would require additional regional data gathering and synthesis for a watershed of this scale. The use of a formal Bayesian approach (Viglione et al., 2013) to combine the information sources and models presented here is also worthwhile. Reclamation is expanding detailed paleoflood data and storm rainfall data collection at other critical facilities where hydrologic risks indicate the need for new data for flood hazard estimation.

Acknowledgments

Funding for this study was provided partially by the Bureau of Reclamation's Dam Safety Office and Science and Technology Program in Denver, and the Department of Defense through the Center for Geosciences at Colorado State University. We acknowledge comments from an anonymous reviewer and Dr. Alberto Viglione that helped us clarify several points and improve this paper. The TREX model source code is freely available from the authors.

Appendix A. Supplementary material

Supplementary animations of water depth estimates (in meters) from the TREX model for the unrestricted rainfall and restricted rainfall cases, corresponding to the largest runoff event, can be found in the online version at http://dx.doi.org/10.1016/j.jhydrol.2013.12.021.

References

Alexander, G.N., 1963. Using the probability of storm transposition for estimating the frequency of rare floods. J. Hydrol. 1, 46–57.

Benito, G., Ouarda, T.B.M.J., Bárdossy, A., 2005. Applications of palaeoflood hydrology and historical data in flood risk analysis. J. Hydrol. 313 (1–2), 1–2. http://dx.doi.org/10.1016/j.jhydrol.2005.02.001.

Beven, K.J., 2001. Rainfall–Runoff Modeling, The Primer. John Wiley and Sons, Chichester, 360p.

Blazkova, S., Beven, K.J., 2002. Flood frequency estimation by continuous simulation for a catchment treated as ungaged (with uncertainty). Water Resour. Res. 38 (8), 14-1–14-14. http://dx.doi.org/10.1029/2001WR000500.

Blazkova, S., Beven, K.J., 2004. Flood frequency estimation by continuous simulation of subcatchment rainfalls and discharges with the aim of improving dam safety assessment in a large basin in the Czech Republic. J. Hydrol. 292, 153–172.

Burges, S.J., 1998. Streamflow prediction: capabilities, opportunities and challenges. In: Hydrologic Sciences: Taking Stock and Looking Ahead. National Research Council, Washington, DC, pp. 101–134.

Cameron, D., 2007. Flow, frequency, and uncertainty estimation for an extreme historical flood event in the Highlands of Scotland, UK. Hydrol. Process. 21, 1460–1470.

Cameron, D.S., Beven, K.J., Tawn, J., Blazkova, S., Naden, P., 1999. Flood frequency estimation by continuous simulation for a gaged upland catchment (with uncertainty). J. Hydrol. 219, 169–187.

Cameron, D.S., Beven, K.J., Tawn, J., Blazkova, S., Naden, P., 2000. Flood frequency estimation by continuous simulation (with likelihood based uncertainty estimation). Hydrol. Earth Syst. Sci. 4 (1), 23–34.

Cohn, T.A., Lane, W.L., Baier, W.G., 1997. An algorithm for computing moments-based flood quantile estimates when historical information is available. Water Resour. Res. 33 (9), 2089–2096.

Cohn, T.A., Lane, W.L., Stedinger, J.R., 2001. Confidence intervals for EMA flood quantile estimates. Water Resour. Res. 37 (6), 1695–1706.

Cordova, J.R., Rodriguez-Iturbe, I., 1983. Geomorphoclimatic estimation of extreme flow probabilities. J. Hydrol. 65, 159–173.

Cudworth Jr., A.G., 1989. Flood Hydrology Manual. A Water Resources Technical Publication. U.S. Department of Interior, Bureau of Reclamation, Denver, Colorado, 243p.

Doesken, N.J., 1991. General climatology in colorado. In: Paulson, R.W., Chase, E.B., Roberts, R.S., Moody, D.W. (compilers), National Water Summary 1988-89-Hydrologic Events and Floods and Droughts, U.S. Geological Survey Water-Supply Paper 2375, pp. 207–208.

Doesken, N.J., 1998. A Post-evaluation of Rainfall Reports Associated with the Pawnee Creek flood of July 29–30, 1997 in Eastern Weld and Western Logan Counties in Northeast Colorado, Climatology Report #98-3, Department of Atmospheric Science, Colorado State University, Fort Collins, Colorado, 33p.

Doesken, N.J., McKee, T.B., 1998. An Analysis of Rainfall for the July 28, 1997 Flood in Fort Collins, Colorado, Climatology Report #98-1, Department of Atmospheric Science, Colorado State University, Fort Collins, Colorado, 55 p.

Dunne, T., 1998. Wolman lecture: hydrologic science … in landscapes … on a planet … in the future. In: Hydrologic Sciences: Taking Stock and Looking Ahead. National Research Council, Washington, DC, pp. 10–43.

Deutsche Vereinigung für Wasserwirtschaft, Abwasser und Abfall (DWA) 2012. Ermittlung von Hochwasserwahrscheinlichkeiten (Determination of Flood Probabilities), Tech. Rep. DWA-M. 552, Hennef, Germany.

England, Jr. J.F., 2006. Frequency Analysis and Two-dimensional Simulations of Extreme Floods on a Large Watershed. Ph.D. Dissertation, Department of Civil Engineering, Colorado State Univ., Fort Collins, Colorado, 237p.

England Jr., J.F., 2011. Flood frequency and design flood estimation procedures in the United States: progress and challenges. Aust. J. Water Res. 15 (1), 33–46.

England, Jr., J.F., Klawon, J.E., Klinger, R.E., Bauer, T.R., 2006. Flood Hazard Study, Pueblo Dam, Colorado, Final Report, Bureau of Reclamation, Denver, CO, June, 160 p.

England Jr., J.F., Velleux, M.L., Julien, P.Y., 2007. Two-dimensional simulations of extreme floods on a large watershed. J. Hydrol. 347 (1–2), 229–241. http://dx.doi.org/10.1016/j.jhydrol.2007.09.034.

England Jr., J.F., Nicholson, T.J., Prasad, R., 2008. Extreme storm event assessments for nuclear facilities and dam safety. EOS, Trans. AGU 89 (53), Fall Meet. Suppl., Abstract H13D-0954.

England Jr., J.F., Godaire, J.E., Klinger, R.E., Bauer, T.R., Julien, P.Y., 2010. Paleoflood hydrology and extreme flood frequency of the Upper Arkansas River, Colorado, USA. Geomorphology 124, 1–16. http://dx.doi.org/10.1016/j.geomorph.2010.07.021.

Fiorentino, M., Iacobellis, V., 2001. New insights about the climatic and geologic control on the probability distribution of floods. Water Resour. Res. 37 (3), 721–730.

Follansbee, R., Jones, E.E., 1922. Arkansas River Flood of June 3–5, 1921, U.S. Geological Survey Water-Supply Paper 487, 44p.

Follansbee, R., Sawyer, L.R., 1948. Floods in Colorado, U.S. Geological Survey Water-Supply Paper 997, 151p.

Fontaine, T.A., Potter, K.W., 1989. Estimating probabilities of extreme rainfalls. J. Hydraul. Engr. ASCE 115 (11), 1562–1575.

Foufoula-Georgiou, E., 1989. A probabilistic storm transposition approach for estimating exceedance probabilities of extreme precipitation depths. Water Resour. Res. 25 (5), 799–815.

Foufoula-Georgiou, E., Wilson, L.L., 1990. In search of regularities in extreme rainstorms. J. Geophys. Res. 95 (D3), 2061–2072.

Franchini, M., Helmlinger, K.R., Foufoula-Georgiou, E., Todini, E., 1996. Stochastic storm transposition coupled with rainfall–runoff modeling for estimation of exceedance probabilities of design floods. J. Hydrol. 175 (1–4), 511–532.

Fuller, W.E., 1914. Flood flows. Trans. Am. Soc. Civ. Eng. 77, 564–617, Paper No. 1293.

Fuller, M.L., 1917. Discussion of the final report of the special committee on floods and flood prevention. Trans. Am. Soc. Civ. Eng. 81, 1269–1278, Paper No. 1400.

Gutknecht, D., Blöschl, G., Reszler, Ch., Heindl, H., 2006. Ein "Mehr-Standbeine" Ansatz zur Ermittlung von Bemessungshochwässern kleiner Auftretenswahrscheinlichkeit (A "multi-pillar"-approach to the estimation of low probability design floods). Österr. Wasser Abfallwirtsch. 58 (3/4), 44–50.

Hansen, E.M., Schreiner, L.C., Miller, J.F., 1982. Application of Probable Maximum Precipitation Estimates-United States East of the 105th Meridian. Hydrometeorological Report No. 52, National Weather Service, Washington, DC, 168p.

Hansen, E.M., Fenn, D.D., Schreiner, L.C., Stodt, R.W., Miller, J.F., 1988. Probable Maximum Precipitation Estimates-United States between the Continental Divide and the 103rd Meridian. Hydrometeorological Report No. 55A, National Weather Service, National Oceanic and Atmospheric Administration, U.S. Department of Commerce, Silver Spring, MD, 242p.

Hashemi, A.M., Franchini, M., O'Connell, P.E., 2000. Climate and basin factors affecting the flood frequency curve: PART I – a simple sensitivity analysis based on the continuous simulation approach. Hydrol. Earth Syst. Sci. 4 (3), 463–482.

Hazen, A.M., 1914. Discussion of Flood flows by W.E. Fuller. Trans. Am. Soc. Civ. Eng. 77, 626–632, Paper No. 1293.

Hydrologic Engineering Center (HEC), 2010. Hydrologic Modeling System HEC-HMS, User's Manual, CPD-74A, version 3.5, U.S. Army Corps of Engineers, Davis, CA, 306p.

Hirsch, R.M., Stedinger, J.R., 1987. Plotting positions for historical floods and their precision. Water Resour. Res. 23 (4), 715–727.

Hosking, J.R.M., Wallis, J.R., 1997. Regional Frequency Analysis – An Approach based on L-Moments. Cambridge University Press, 224p.

House, P.K., Webb, R.H., Baker, V.R., Levish, D.R. (Eds.), 2002. Ancient Floods. Modern Hazards: Principles and Applications of Paleoflood Hydrology, Water Sciences and Application, vol. 5. American Geophysical Union, Washington DC, p. 385p.

Huff, F.A., 1967. Time distribution of rainfall in heavy storms. Water Resour. Res. (4), 1007–1019.

Iacobellis, V., Fiorentino, M., 2000. Derived distribution of floods based on the concept of partial area coverage with a climatic appeal. Water Resour. Res. 36 (2), 469–482.

Jarrett, R.D., 1987. Flood Hydrology of Foothill and Mountain Streams in Colorado. Ph.D. Dissertation, Department of Civil Engineering, Colorado State Univ., Fort Collins, Colorado, 239p.

Jarrett, R.D., 1990. Paleohydrologic techniques used to define the spatial occurrence of floods. Geomorphology 3, 181–195.

Jarrett, R.D., 1993. Flood elevation limits in the Rocky Mountains. In: Kuo, C.Y. (Ed.), Engineering Hydrology-Proceedings of the symposium sponsored by the Hydraulics Division, ASCE, July 25–30, 1993, San Francisco, CA, pp. 180–185.

Jarrett, R.D., England Jr., J.F., 2002. Reliability of paleostage indicators for paleoflood studies. In: House, P.K., Webb, R.H., Baker, V.R., Levish, D.R. (Eds.), Ancient Floods, Modern Hazards: Principles and Applications of Paleoflood Hydrology, Water Sciences and Application, vol. 5. American Geophysical Union, Washington DC, pp. 91–109.

Javier, J.R., Smith, J.A., England, J., Baeck, M.L., Steiner, M., Ntelekos, A.A., 2007. The climatology of extreme rainfall and flooding from orographic thunderstorm systems in the upper Arkansas River Basin. Water Resour. Res. 43 (10), W10410. http://dx.doi.org/10.1029/2006WR00509, 13p.

Klinger, R.E., Klawon, J.E., 2002. Development of a Paleoflood Database for Rivers in the Western U.S., Bureau of Reclamation, Denver, CO, 38p.

Koutsoyiannis, D., Foufoula-Georgiou, E., 1993. A scaling model of a storm hyetograph. Water Resour. Res. 29 (7), 2345–2361.

Laurenson, E.M., Mein, R.G., Nathan, R.J., 2006. RORB Version 5 Runoff Routing Model – User Manual, Department of Civil Engineering, Monash University.
Levish, D.R., 2002. Paleohydrologic bounds: nonexceedance information for flood hazard assessment. In: House, P.K., Webb, R.H., Baker, V.R., Levish, D.R. (Eds.), Ancient Floods, Modern Hazards: Principles and Applications of Paleoflood Hydrology, Water Sciences and Application, vol. 5. American Geophysical Union, Washington DC, pp. 175–190.
Levish, D.R., England Jr. J.F., Klawon, J.E., O'Connell, D.R.H., 2003. Flood Hazard Analysis for Seminoe and Glendo Dams, Kendrick and North Platte Projects, Wyoming, Final Report, Bureau of Reclamation, Denver, CO, 126p.
Mahoney, K., Alexander, M.A., Thompson, G., Barsugli, J.J., Scott, J.D., 2012. Changes in hail and flood risk in high-resolution simulations over Colorado's mountains. Nature Clim. Change (2), 125–131. http://dx.doi.org/10.1038/nclimate1344.
Marco, J.B., Valdés, J.B., 1998. Partial area coverage distribution for flood frequency analysis in arid regions. Water Resour. Res. 34 (9), 2309–2317.
McKee, T.B., Doesken, N.J., 1997. Colorado Extreme Storm Precipitation Data Study, Climatology Report #97-1, Department of Atmospheric Science, Colorado State University, Fort Collins, Colorado, 34p (and appendices).
Merz, R., Blöschl, G., 2008a. Flood frequency hydrology: 1. Temporal, spatial, and causal expansion of information. Water Resour. Res. 44, W08432. http://dx.doi.org/10.1029/2007WR006744.
Merz, R., Blöschl, G., 2008b. Flood frequency hydrology: 2. Combining data evidence. Water Resour. Res. 44, W08433. http://dx.doi.org/10.1029/2007WR006745.
Moon, J., Kim, J.-H., Yoo, C., 2004. Storm-coverage effect on dynamic flood frequency analysis: empirical data analysis. Hydrol. Process. 18, 159–178.
Munn, J., Savage, J.L., 1922. The flood of June 1921 in the Arkansas River, at Pueblo, Colorado. Trans. Am. Soc. Civ. Eng. 85, 1–35, with discussion pp. 36–65.
Naghettini, M., Potter, K.W., Illangasekare, T., 1996. Estimating the upper tail of flood-peak frequency distributions using hydrometeorological information. Water Resour. Res. 32 (6), 1729–1740. http://dx.doi.org/10.1029/96WR00200.
Nathan, R.J., Weinmann, P.E., 1999. Estimation of Large to Extreme Floods: Book VI in Australian Rainfall and Runoff. A Guide to Flood Estimation. The Institution of Engineers, Australia.
National Research Council (NRC), 1988. Estimating Probabilities of Extreme Floods: Methods and Recommended Research. National Academy Press, Washington, DC, 141p.
National Research Council (NRC), 1994. Estimating Bounds on Extreme Precipitation Events: A Brief Assessment. National Academy Press, Washington, DC, 29p.
Nicótina, L., Alessi Celegon, E., Rinaldo, A., Marani, M., 2008. On the impact of rainfall patterns on the hydrologic response. Water Resour. Res. 44, W12401. http://dx.doi.org/10.1029/2007WR006654.
O'Connell, D.R.H., Ostenaa, D.A., Levish, D.R., Klinger, R.E., 2002. Bayesian flood frequency analysis with paleohydrologic bound data. Water Resour. Res. 38 (5), 16-1–16-14.
Ponce, V.M., 1989. Engineering Hydrology. Prentice-Hall, NJ, 640p.
U.S. Department of Interior, Bureau of Reclamation (Reclamation), 2002. Flood Hazard Analysis – Folsom Dam, Central Valley Project, California, Bureau of Reclamation, Denver, CO, 128p.
U.S. Department of Interior, Bureau of Reclamation (Reclamation), 2010. Dam Safety Risk Analysis Best Practices Training Manual, version 2.1, Bureau of Reclamation, Denver, Colorado.
U.S. Department of Interior, Bureau of Reclamation (Reclamation), 2011. Dam Safety Public Protection Guidelines, A Risk Framework to Support Dam Safety Decision-Making, Bureau of Reclamation, Denver, Colorado, 31p.
Rogger, M., Kohl, B., Pirkl, H., Viglione, A., Komma, J., Kirnbauer, R., Merz, R., Blöschl, G., 2012. Runoff models and flood frequency statistics for design flood estimation in Austria Do they tell a consistent story? J. Hydrol., 456–457. http://dx.doi.org/10.1016/j.jhydrol.2012.05.068, 30-43.
Sankovich, V., Caldwell, R.J., 2011. Extreme Storm Data Catalog Development, Research Report DSO-11-07. Bureau of Reclamation, Denver, CO, 40p.
Schreiner, L.C., Riedel, J.T., 1978. Probable Maximum Precipitation Estimates, United States East of the 105th Meridian. Hydrometeorological Report No. 51, National Weather Service, National Oceanic and Atmospheric Administration, U.S. Department of Commerce, Silver Spring, MD, 87p.
Schumann, A.H. (Ed.), 2010. Flood Risk Assessment and Management: How to Specify Hydrological Loads, Their Consequences and Uncertainties. Springer, New York, p. 79p.
Stedinger, J.R., Vogel, R.M., Foufoula-Georgiou, E., 1993. Frequency analysis of extreme events. In: Maidment, D.R. (Ed.), Handbook of Hydrology. McGraw-Hill, New York, pp. 18.1–18.6 (Chapter 18).
Struthers, I., Sivapalan, M., 2007. A conceptual investigation of process controls upon flood frequency: role of thresholds. Hydrol. Earth Syst. Sci. 11, 1405–1416.
Swain, R.E., England Jr., J.F., Bullard, K.L., Raff, D.A., 2006. Guidelines for Evaluating Hydrologic Hazards. Bureau of Reclamation, Denver, CO, 83p.
U.S. Army Corps of Engineers (USACE), 1973. Storm Rainfall in the United States, 1945–1973, Washington, D.C.
Velleux, M., Julien, P.Y., Rojas-Sanchez, R., Clements, W.H., England, J., 2006. Simulation of metals transport and toxicity at a mine-impacted watershed: California Gulch, Colorado. Environ. Sci. Technol. 40 (22), 6996–7004.
Velleux, M., England, J.F., Julien, P.Y., 2008. TREX: spatially distributed model to assess watershed contaminant transport and fate. Sci. Total Environ. 404 (1), 113–128.
Velleux, M., England, J.F., Julien, P.Y., 2011. TREX Watershed Modeling Framework User's Manual: Model Theory and Description, Department of Civil Engineering, Colorado State Univ., Fort Collins, January, 106p. <http://www.engr.colostate.edu/pierre/ce_old/Projects/TREX%20Web%20Pages/TREX-Home.html>.
Viglione, A., Merz, R., Blöschl, G., 2009. On the role of the runoff coefficient in the mapping of rainfall to flood return periods. Hydrol. Earth Syst. Sci. 13, 577–593.
Viglione, A., Merz, R., Salinas, J.L., Blöschl, G., 2013. Flood frequency hydrology: 3. A Bayesian analysis. Water Resour. Res. 49. http://dx.doi.org/10.1029/2011WR010782.
U.S. Department of Interior, Water and Power Resources Service, 1981. Project Data, A Water Resources Technical Publication, Denver, Colorado.
Wilson, L.L., 1989. Assessment of the Exceedance Probability of Extreme Rainfalls in the Midwest by Stochastic Storm Transposition. M.S. Thesis, Iowa State University, Ames, IA, 127p.
Wilson, L.L., Foufoula-Georgiou, E., 1990. Regional rainfall frequency analysis via stochastic storm transposition. J. Hydraul. Engr. ASCE 116 (7), 859–880.
Woolhiser, D.A., Smith, R.E., Giraldez, J.-V., 1996. Effects of spatial variability of saturated hydraulic conductivity on Hortonian overland flow. Water Resour. Res. 32 (3), 671–678.